POLITECNICO DI TORINO

Dipartimento di Ingegneria Meccanica ed Aerospaziale
Corso di Laurea in Ingegneria Aerospaziale

Tesi di Laurea Magistrale

Design of attitude control algorithms for a spinning CubeSat using magnetorquers

Relatore
prof. Sabrina Corpino

Candidato
Davide Carabellese

Tutor
prof. Mason A. Peck

Luglio 2018

Contents

List of Figures

List of Tables

Abstract

The purpose of this thesis is to develop and simulate different algorithms for the ACS of a spinning CubeSat using magnetorquers and the interaction with the Earth's magnetic field. This work has been developed within the Cornell University Space Systems Design Studio (SSDS) during the design process of the Alpha CubeSat together with a Team of students at Cornell University, for which the developed ACS has been designed. The work is divided in three main phases: the control design, the stability analysis and the simulation phase. In particular for this purpose, two algorithms to align the angular momentum vector with the maximum principal axis of inertia have been studied. The first is a classical approach, using a B-dot like algorithms to damp the transversal components of the angular velocity. The second algorithm uses an fictional model based on energy dissipation principle to elaborate an algorithm for damping the transversal components of the angular momentum, based on the T. R. Kane work on the effects of energy dissipation on a spinning CubeSat. The latter algorithm is used in the ACS controller, since it doesn't require a precise knowledge of the spacecraft's inertia matrix. After assessing a stable spinning condition, another linear Proportional-Derivative algorithm is used to align the spin axis with the Earth's magnetic field. For the aforementioned algorithms linear and nonlinear stability analysis have been evaluated, based on root locus methods and frequency response for the linear and linearized controllers and using the Lyapunov's method for the nonlinear control algorithms. The simulations have been pursued with the use of MATLAB Simulink package. The results highlight the strength of the chosen algorithms for unknown initial conditions and also show the time performance of the proposed solution. In particular they show how, regardless of the initial condition, the first algorithm is able to detumble the spacecraft and spin it about the axis of maximum inertia and the second algorithm is able to align the spin axis with the magnetic field lines with a precision under 10 degrees.

Sommario

Lo scopo di questa tesi è quello di sviluppare e simulare diversi algoritmi per l' ACS di un CubeSat in rotazione intorno al proprio asse di massima inerzia, con l' utilizzo di dipoli magnetici e l'interazione con il campo magnetico terrestre. Il presente lavoro è stato sviluppato all'interno dello Space System Design Studio (SSDS) durante la fase di design dell' Alpha CubeSat con un team di studenti presso la Cornell University, per il quale l' ACS è stato progettato. Il lavoro è diviso principalmente in tre fasi: la fase di control design, l'analisi di stabilità e la fase di simulazione. In particolare per questo scopo, sono stati studiati due algoritmi per allineare il vettore del momento angolare con l' asse di massima inerzia. Il primo utilizza un approccio classico, utilizzando un algoritmo simile al B-dot, per smorzare le componenti trasversali della velocità angolare. Il secondo algoritmo utilizza un modello fittizio basato sul principio di dissipazione dell' energia per elaborare un algoritmo in grado di smorzare le componenti trasversali di momento angolare, basato sul lavoro di T. R. Kane sugli effetti della dissipazione energetica su un CubeSat rotante. L'ultimo algoritmo è stato utilizzato nel ACS, avendo il vantaggio di non necessitare una precisa conoscenza della matrice di inerzia dello spacecraft. Dopo aver assicurato una condizione di rotazione stabile, viene utilizzato un'altro algoritmo proporzionale-derivativo per allineare l' asse di rotazione con le linee di campo magnetico terrestre. Per i soprammenzionati algoritmi è stata valutata la stabilità, lineare e non lineare, tramite il metodo del root locus e risposta in frequenza nel caso lineare ed utilizzando il metodo di Lyapunov per l'analisi non lineare. Infine le simulazioni sono state effettuate con l' utilizzo del pacchetto Simulink di MATLAB. I risultati evidenziano i punti di forza degli algoritmi utilizzati, per condizioni iniziali incognite, e mostrano le performance della soluzione proposta. In particolare si vede come il primo algoritmo sia in grado di smorzare le componenti trasversali di velocità e portare il satellite in uno stato di spin alla velocità angolare desiderata, mentre il secondo algoritmo è in grado di allineare l'asse di spin con le linee di campo magnetico con una precisione al di sotto dei 10 gradi.

Chapter 1

Introduction

1.1 CubeSat History

The CubeSat form is a standardized layout of satellite that has begun revolutionizing access to space. Basically it is made up of multiples U units ($10 \times 10 \times 10$ cm cubic units) and its main purpose is for scientific experimentation and low cost mission. Indeed its relatively low costs and brief design process made it the perfect means for testing new technologies and introduce students in the space systems' design. Furthermore, in addition to size limitations, the CubeSats have a mass limitation of 1.33 kilograms per unit, which makes its design process more challenging. In his 2010 TEDxUofM presentation "Making Space Smaller", the CubeSat designer Kiko Dontchev said: "We were given a box and, and we're asking the question: What can we do inside the box?". That's the challenge that every CubeSat design team is asked to deal with. The CubeSat specifications were designed in 1999 by the California Polytechnic State University and Stanford University to promote and develop the skills necessary for the design, manufacture, and testing of small satellites intended for low Earth orbit (LEO) that perform a number of scientific research functions and explore new space technologies. Many CubeSats are used to demonstrate spacecraft technologies that are targeted for use in small satellites or that present questionable feasibility and are unlikely to justify the cost of a larger satellite. That said, CubeSats have come to be a thought of as mission-risk enablers [11] and they are ideal platforms for small scale testing of technologies that can be further qualified and, eventually, reused in a larger scale. Although CubeSats have become ordinary in the aerospace field, the design of its attitude control system is still the main reason of many research.

Their limited size and the low cost, that are the driving factors and the limitations of its entire design process, make designing the Attitude Control System more difficult.

1.2 Alpha CubeSat

The Alpha CubeSat, for which the ACS has been designed, is a 1U CubeSat developed by a Team of students within the Cornell University Space Systems Design Studio (SSDS), under the supervision of the professor Mason Peck. The aforementioned team also participated at the NASA's CubeSat Launch Initiative program (CSLI) which guarantees a launch as piggyback in 2019. The CSLI (similar to ESA's Fly Your Satellite program) provides access to space for small satellites, CubeSats, developed by the NASA Centers and programs, educational institutions and non-profit organizations giving CubeSat developers access to a low-cost pathway to conduct research in the areas of science, exploration, technology development, education or operations. This past March, NASA selected 11 research groups from across the US to partake in their CubeSat launch initiative, which was a project designed to encourage the development of CubeSats or nano-satellites. Two of the 11 projects chosen by NASA for their technological potential were the Pathfinder for Autonomous Navigation (PAN) and Alpha CubeSat, both of which are initiatives from Space Systems Design Studio and both designed and manufactured in Cornell University. The Alpha CubeSat mission is a technology demonstrator with the objective of successfully deploying a light sail for deep space exploration applications such as the Starshot Breakthrough mission. The 1U module consists of a folded sail (potentially 4×4 meters) occupying the upper half of the CubeSat and the spacecraft avionics occupying the remaining half. The sail will be equipped with four Sprite ChipSats on its corners and will be held folded in place by the upper solar panel, acting as a door, secured by a nichrome wire that will be melt when needed to deploy and the deployment is achieved by an hinge with a torsional spring. The unfolding process of the solar sail will be assisted by a nitinol wire that will stretch thanks to the solar heat. To manufacture the CubeSat unit a cutting edge 3D printing technique has been used. The purpose of this Thesis is the design of an Attitude Control System that allows to accomplish the CubeSat primary mission, with the lowest cost and space, for the 1U Alpha CubeSat. After the deployment, the ACS shall spin the satellite about its z-axis, and then pointing that spin axis parallel to the Earth's magnetic field. The spin will assist the light sail on its deployment from the CubeSat. Upon establishing the desired spin rate and orientation, the payload is deployed. Deployment verification is achieved through an on-board camera aligned with the satellite z-axis to get the best view of the deployment. As a backup plan, the deployment may be verified through the reception of the sail's on-board ChipSats' signals. Since the purpose of a CubeSat mission is to be a low cost technological demonstrator, for what concerns the sensors the CubeSat will only be equipped with a three-axis magnetometer and a gyroscope. This reduces the room for maneuver in terms of pointing since we cannot have a proper attitude determination unless we include a Kalman filter for attitude estimation. But, as stated in the mission and system requirements, there's no need to include that since the purpose of the Alpha CubeSat doesn't have any pointing requirements other than aligning the spin axis with the Earth's magnetic field.

1.3 Requirements

In this section we will recall and summarize the driving factors in the design process. Those have been highlighted by the team members in the definition of the Mission Success Criteria and the System Requirements. The work on the ACS is done to satisfy the System Requirements taken taken from the Alpha Verification Requirements Cross Matrix [7] previously written by Team members, hereafter highlighted:

AC&N-1	The CubeSat shall be capable of detumbling the CubeSat.
AC&N-2	The CubeSat shall align its z-axis with magnetic north and have an angular motion about its z-axis during normal operations.
AC&N-3	The CubeSat shall be capable of measuring its orientation and angular velocity.
AC&N-4	The CubeSat shall be capable of measuring its position and linear velocity.
AC&N-5	The attitude determination software shall process the current data from all sensors when determining orientation.

AC&N-6	The attitude determination software shall autonomously solve for all attitude adjustments.
AC&N-7	The AC&N subsystem shall have two control methods: detumbling and normal operation (pointing).
AC&N-8	The AC&N subsystem shall orient the CubeSat z-axis to within 10°. (Earth's Magnetic Field Variation Worst-case)

Table 1.1: System Requirements.

In addition to spin-stabilize the satellite, the successive goal is to orient the spin axis. For what concerns the mission, we'll recall the Mission Success Criteria, that have been the driving factors in defining the ACS system requirements From the Mission Success Criteria [6] the CubeSat shall:

MSC-1	Deploy and verify deployment of the 1×1 m light sail and Sprite picosatellite payload from the CubeSat bus in LEO with an angular rotation about the CubeSat's Z-axis
MSC-1.1	Basic performance goal - demonstrate the CubeSat's ability to deliver the payload to orbit and allow for the payload to unfold. Separation of the payload from the CubeSat bus demonstrates initial success of the CubeSat mission by allowing the payload the opportunity to unfold and achieve complete mission success
MSC-2	Capture at minimum one image of the payload deployment and transmit the image back to Earth
MSC-2.1	Advanced performance goal - demonstrate the payload can unfold once deployed, as well as, get visual confirmation that the payload successfully deployed with the correct orientation. This will be complete mission success if the CubeSat successfully deploys the payload and takes at least one image
MSC-3	Extended Mission: The Sprite Satellite payload shall transmit data back to ground

MSC-3.1	Payload performance goal - demonstrate the Sprite picosatellite can power on and transmit data to the ground using its communication system. This higher level of mission success is indicative of a fully successful mission, demonstrating the Sprite picosatellite's capabilities, which is beyond what the mission intends to show

Table 1.2: Mission Success Criteria.

Chapter 2

Mathematical Modeling

Before starting with the proper control design, lets introduce some mathematical models used for the dynamics and kinematics of the spacecraft, as well as the models and assumptions used for the environment and the inertia of the spacecraft itself.

2.1 Reference frames

Spacecraft are free bodies, possessing both translational and rotational motion. The translational component is the subject of *orbital dynamics*, the rotational component is the subject of *attitude dynamics*. For computational purpose and to describe the orientation of the spacecraft, we need to introduce some useful reference frames. In particular for describing the attitude of a satellite, different frame systems are used. Our coordinate axes consist of two inertial frame axes and one body frame axis.

2.1.1 Earth Centered Inertial frame (ECI)

This frame system is a non-spin coordinate system in a fixed space, denoted by the unit vectors IJK. The ECI coordinate system is typically defined as a Cartesian coordinate system, where the coordinates (position) are defined as the distance from the origin along the three orthogonal (mutually perpendicular) axes. The z axis runs along the Earth's rotational axis pointing North, the x axis points in the direction of the vernal equinox (more on this in a moment), and the y axis completes the right-handed orthogonal system. As seen in Figure 2.1, the vernal equinox is an imaginary point in space which lies along the line representing the intersection of the Earth's equatorial plane and the plane of the Earth's orbit around the Sun or the ecliptic. Another way of thinking of the x axis is that it is the line segment pointing from the center of the Earth towards the center of the Sun at the beginning of Spring, when the Sun crosses the Earth's equator moving North. The x axis, therefore, lies in both the equatorial plane and the ecliptic. These three axes defining the Earth-Centered Inertial coordinate system are 'fixed' in space and do not rotate with the Earth.

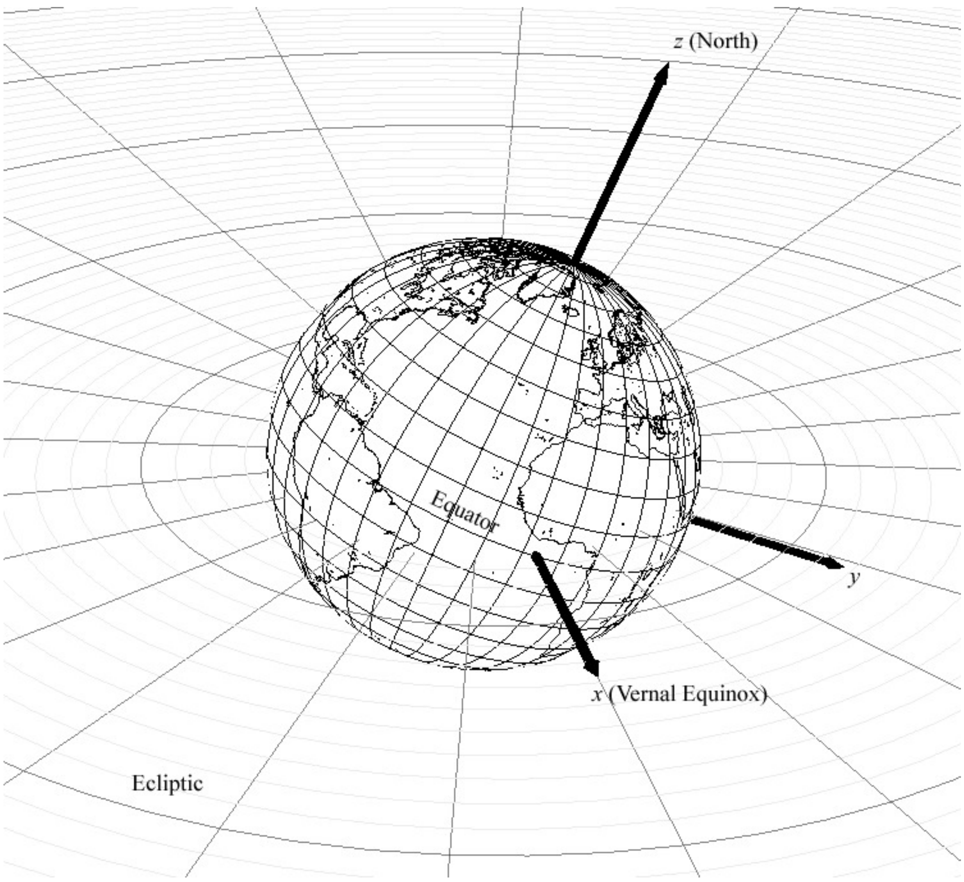

Figure 2.1: ECI reference frame.

2.1.2 Perifocal coordinate system (PQW)

Another useful frame is the P,Q,W frame where $\overline{P}$ and $\overline{Q}$ are unit vectors in the orbit plane, with $\overline{P}$ directed to perigee, $\overline{W}$ along the angular momentum vector and $\overline{Q}$ completing a right hand triad, i.e., $\overline{P} \times \overline{Q} = \overline{W}$. This reference frame is useful to define the initial condition and the position of the spacecraft along its orbit and then to identify its position and velocity with respect to the inertial frame. The Euler angles Ω, ω and i are used to describe the orientation of these axes with respect to the ECI frame. Ω is the Right Ascension of the Ascending Node (RAAN). The angle i is the inclination, the angle between the orbital plane and the XY plane of the ECI fame. The angle ω is called the argument of periapsis. To go from IJK (ECI) to PQW we first rotate about the K axis through Ω. Next rotate about the new X-axis through i, the inclination, then rotate about the resulting Z-axis through ω. The rotation matrices from ECI to PWQ are defined as follows:

$$\begin{bmatrix} P \\ W \\ Q \end{bmatrix} = \begin{bmatrix} c_\omega & s_\omega & 0 \\ -s_\omega & c_\omega & 0 \\ 0 & 0 & 1 \end{bmatrix} \begin{bmatrix} 1 & 0 & 0 \\ 0 & c_i & s_i \\ 0 & -s_i & c_i \end{bmatrix} \begin{bmatrix} c_\Omega & s_\Omega & 0 \\ -s_\Omega & c_\Omega & 0 \\ 0 & 0 & 1 \end{bmatrix} \begin{bmatrix} X_I \\ Y_I \\ Z_I \end{bmatrix}$$

or

$$\begin{bmatrix} P \\ W \\ Q \end{bmatrix} = \begin{bmatrix} c_\omega c_\Omega & -s_\omega c_i s_\Omega & s_\omega s_i \\ -s_\omega c_\Omega & -c_\omega c_i s_\Omega & c_\omega s_i \\ s_i s_\Omega & -s_i c_\Omega & c_i \end{bmatrix} \begin{bmatrix} X_I \\ Y_I \\ Z_I \end{bmatrix} \tag{2.1}$$

where c and s represent respectively the cosine and the sine of the subscript angle and the matrix in (2.1) is the rotation matrix between the two coordinate frames.

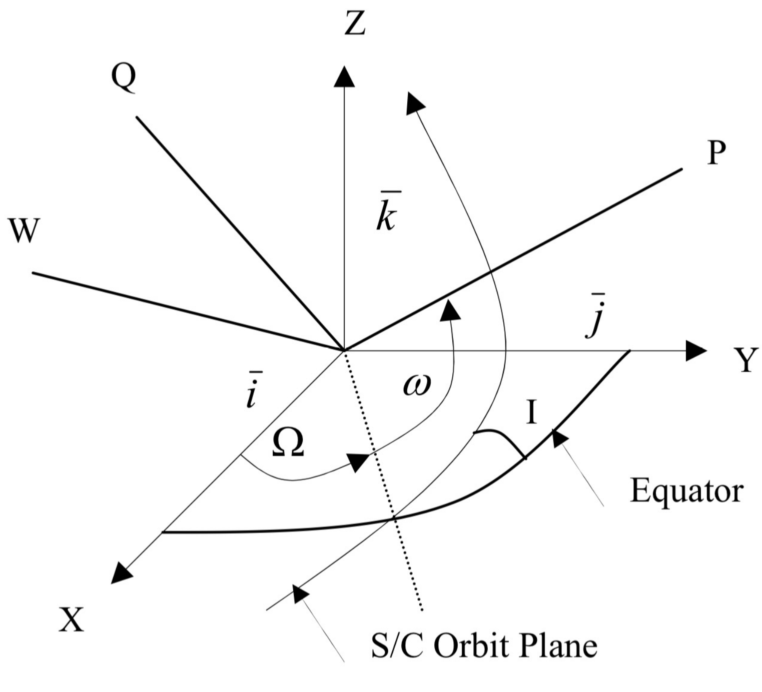

Figure 2.2: PWQ reference frame.

2.1.3 Body coordinate system

The spacecraft body frame is a set of three vectors attached to the body of the spacecraft allowing the frame to rotate with the spacecraft. The frame origin is located at the center of mass of the spacecraft, to simplify rotational characteristics of the body in free-space. Under rigid-body conditions, each discrete component of the spacecraft can be defined by vector from the spacecraft center of mass and does not change with respect to time. In our configuration, the z-axis is oriented in the direction of the spin axis (the roll axis) and the x and y axis are oriented perpendicularly to two adjacent lateral faces and complete the right-handed orthogonal system as shown in Figure 2.3.

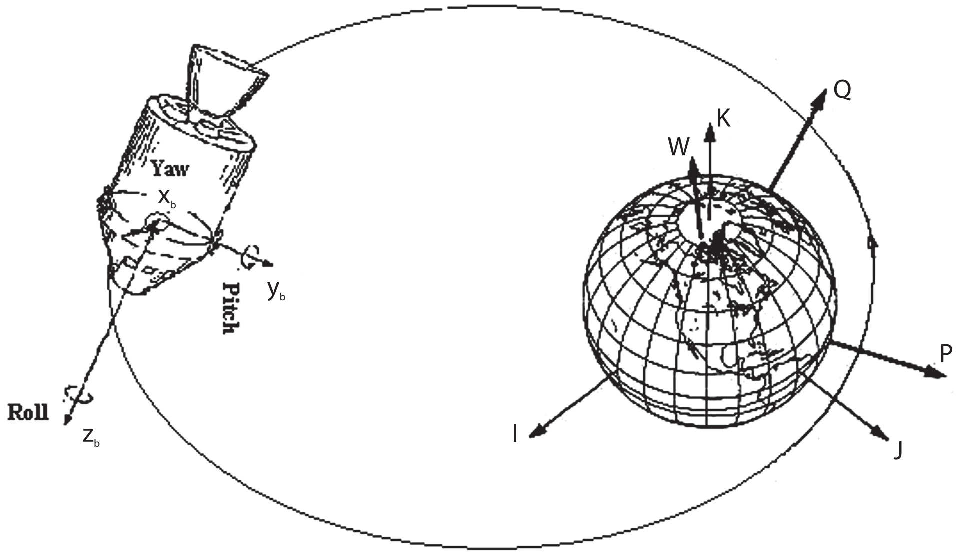

Figure 2.3: ECI, PQW and body reference frames.

2.2 Spacecraft kinematics and dynamics

While the spacecraft moves into space, it is subject to external forces and it will respond with well-known physical principles that can be measured and controlled. We will now introduce the spacecraft Kinematics and Dynamics principles and their mathematical formulation.

2.2.1 Kinematics

When talking about the attitude of the spacecraft, it only makes sense if it is relative to something, i.e. an inertial frame ($\mathcal{F}_n$. The attitude can be fully described by outlining the orientation of a reference frame attached to the spacecraft, i.e. $\mathcal{F}_b$ body-fixed frame, with respect to the inertial frame. This orientation, thus the attitude, is fully described by a rotation matrix $\mathbf{C}_{bn}$ as well as an Euler rotation sequence or quaternions (known as Euler parameters). We may use a 3-2-1 Euler rotation sequence, given by:

1. A rotation ψ about the original z-axis (yaw);

2. A rotation θ about new y-axis (pitch);

3. A rotation φ about final x-axis (roll);

These angles equivalently represent the attitude. Indeed they are also used in the rotation matrix $\mathbf{C}_{bn}$:

$$\mathbf{C}_{bn}(\psi,\theta,\varphi) = \begin{bmatrix} c_\theta c_\psi & c_\theta s_\psi & -s_\theta \\ s_\varphi s_\theta c_\psi - c_\varphi s_\psi & s_\varphi s_\theta s_\psi + c_\varphi c_\psi & s_\varphi c_\theta \\ c_\varphi s_\theta c_\psi + s_\varphi s_\psi & c_\varphi s_\theta s_\psi - s_\varphi c_\psi & c_\varphi c_\theta \end{bmatrix} \tag{2.2}$$

where $s_b = \sin b$ and $c_b = \cos b$. Given any rotation matrix $\mathbf{C}_{bn}$, the corresponding Euler angles may be determined, unless the rotation matrix corresponds to the singularity Euler sequence (when θ
$pm90°$ for the 3-2-1 Euler sequence) also known as Gimbal Lock. Any Euler sequence has its singularity. To avoid this singularity we can use the direct cosine matrix or the quaternion four-parameter representation of the attitude. In general, the axis of rotation will not be one of the reference axes. In terms of the unit vector along the rotation axis $\hat{e}$, and angle of rotation, Φ, the most general direction cosine matrix[27] is:

$$A = \begin{bmatrix} \cos\Phi + e_1^2(1-\cos\Phi) & e_1e_2(1-\cos\Phi) + e_3\sin\Phi & e_1e_3(1-\cos\Phi) - e_2\sin\Phi \\ e_1e_2(1-\cos\Phi) - e_3\sin\Phi & \cos\Phi + e_2^2(1-\cos\Phi) & e_2e_3(1-\cos\Phi) + e_1\sin\Phi \\ e_1e_3(1-\cos\Phi) + e_2\sin\Phi & e_2e_3(1-\cos\Phi) - e_1\sin\Phi & \cos\Phi + e_3^2(1-\cos\Phi) \end{bmatrix} =$$

$$= \cos\Phi\mathbf{1} + (1-\cos\Phi)\hat{e}\hat{e}^T - \sin\Phi e^\times \tag{2.3}$$

where $\hat{e}\hat{e}^T$ is the outer product and $e^\times$ is the skew anti-symmetric matrix defined as:

$$e^\times = \begin{bmatrix} 0 & -e_3 & e_2 \\ e_3 & 0 & -e_1 \\ -e_2 & e_1 & 0 \end{bmatrix} \tag{2.4}$$

A parameterization of the direction cosine matrix in terms of Euler parameters, or quaternions, q_0, q_1, q_2, q_3 has proved to be quite useful in spacecraft applications. They are defined as:

$$q_1 = e_1 \sin\frac{\Phi}{2} \tag{2.5}$$

$$q_2 = e_2 \sin\frac{\Phi}{2} \tag{2.6}$$

$$q_2 = e_3 \sin\frac{\Phi}{2} \tag{2.7}$$

$$q_0 = \cos\frac{\Phi}{2} \tag{2.8}$$

$$\tag{2.9}$$

where the first three parameters represent the vectorial part of quaternion and the last one is a scalar:

$$\mathbf{q} = \begin{bmatrix} \vec{\boldsymbol{\epsilon}} \\ \eta \end{bmatrix} = \begin{bmatrix} q_1 \\ q_2 \\ q_3 \\ q_0 \end{bmatrix}$$

The four Euler paramenters are not independent, but satisfy the constraint equation:

$$q_1^2 + q_2^2 + q_3^2 + q_0^2 = 1$$

The direction cosine matrix can be expressed in terms of the Euler symmetric parameters by:

$$A(\mathbf{q}) = \begin{bmatrix} q_1^2 - q_2^2 - q_3^2 + q_0^2 & 2(q_1q_2 + q_3q_0) & 2(q_1q_3 - q_2q_0) \\ 2(q_1q_2 - q_3q_0) & -q_1^2 + q_2^2 - q_3^2 + q_0^2 & 2(q_2q_3 - q_1q_0) \\ 2(q_1q_3 - q_2q_0) & 2(q_2q_3 - q_1q_0) & -q_1^2 - q_2^2 + q_3^2 + q_0^2 \end{bmatrix} =$$

$$= (\eta^2 - \vec{\boldsymbol{\epsilon}}^2)\mathbf{1} + 2\vec{\boldsymbol{\epsilon}}\vec{\boldsymbol{\epsilon}}^T - 2\eta Q \tag{2.10}$$

where Q is defined as (2.4), relative to the vectorial part of the quaternion. All methods are mathematically equivalent, but numerical inaccurancy can be minimized with Euler parameters. Furthermore they are more compact than the DCM because they require only four parameters rather than nine and more convenient than the Euler axis and angle parametrization because the expression for the DCM transformation doesn't require trigonometric functions.
The spacecraft has angular velocity $\vec{\omega}_{bn}$ relative to the inertial frame $\mathcal{F}_n$. If we

express $\tilde{\omega}_b^n$ in the body-fixed frame F_b as

$$\vec{\boldsymbol{\omega}}_b^n = F_b^T \boldsymbol{\omega}_b^n \tag{2.11}$$

the attitude kinematics in terms of the rotation matrix are

$$\dot{\mathbf{C}}_b^n = -\boldsymbol{\omega}_b^n \times \mathbf{C}_{bn} \tag{2.12}$$

Hence the attitude kinematics in terms of Euler 3-2-1 rotation sequence are:

$$\begin{bmatrix} \dot{\psi} \\ \dot{\theta} \\ \dot{\varphi} \end{bmatrix} = \begin{bmatrix} 1 & \sin\psi\tan\theta & \cos\psi\tan\theta \\ 0 & \cos\psi & -\sin\psi \\ 0 & \sin\psi\sec\theta & \cos\psi\sec\theta \end{bmatrix} \boldsymbol{\omega}_b^n \tag{2.13}$$

or in terms of quaternions as:

$$\begin{aligned} \dot{\boldsymbol{\epsilon}} &= \frac{1}{2}\left(\eta\mathbf{1} + \epsilon^{\times}\right)\boldsymbol{\omega}_b^n, \\ \dot{\eta} &= -\frac{1}{2}\boldsymbol{\epsilon}^T\boldsymbol{\omega}_b^n, \end{aligned} \tag{2.14}$$

2.2.2 Dynamics

We can consider the spacecraft as a rigid body and study its dynamics. A rigid body is a continuum in which the distance between any weo points on the body remains fixed. This means that the body does not deform. In particular we will focus on the rotational dynamics rather than the translational ones. We shall refer to the body-fixed reference frame $\mathcal{F}_b$, located in the center of mass of the spacecraft. If we consider the spacecraft as a system of infinite particles, the angular momentum of a system of particles about the center of mass of the spacecraft is:

$$\overrightarrow{h} = \sum_{i=1}^{N} m_i \overrightarrow{\rho_i} \times \overrightarrow{\dot{\rho}_i} = \int_V \overrightarrow{\rho_i} \times \overrightarrow{\dot{\rho}_i}\, dm \tag{2.15}$$

Using the rigid body hypothesis, the inertial time-derivative of $\overrightarrow{\rho}$ is related to the time-derivative of $\overrightarrow{\rho}$ by:

$$\overrightarrow{\dot{\rho}} = \overrightarrow{\mathring{\rho}} + \overrightarrow{\omega} \times \overrightarrow{\rho} \tag{2.16}$$

where $\overrightarrow{\omega}$ is the angular velocity of the rigid body with respect to the inertial frame. Due to the rigid body assumption $\mathring{\rho} = 0$ so we can write:

$$\begin{aligned} \overrightarrow{h} &= \int_V \overrightarrow{\rho} \times (\overrightarrow{\omega} \times \overrightarrow{\rho})\; dm = \\ &= -\int_V \overrightarrow{\rho} \times (\overrightarrow{\rho} \times \overrightarrow{\omega})\; dm = \\ &= \left[-\int_V \overrightarrow{\rho}^{\times}\overrightarrow{\rho}^{\times}\, dm\right]\omega \end{aligned} \tag{2.17}$$

where the quantity in the square brackets is the moment of inertia about the center of mass:

$$\mathbf{I} \triangleq - \int_V \vec{\rho}^{\times} \vec{\rho}^{\times} \, dm =$$

$$= \int_V \begin{bmatrix} (\rho_y^2 + \rho_z^2) & -\rho_x\rho_y & -\rho_x\rho_z \\ -\rho_x\rho_y & (\rho_x^2 + \rho_z^2) & \rho_y\rho_z \\ -\rho_y\rho_z & -\rho_y\rho_z & (\rho_y^2 + \rho_z^2) \end{bmatrix} \sigma(\rho_x, \rho_y, \rho_z) \, dV \tag{2.18}$$

The spacecraft angular momentum about it's center of mass satisfies the equation:

$$\dot{\vec{\mathbf{h}}}_c = \vec{\mathbf{T}}_c \tag{2.19}$$

where $\dot{}$ denotes the inertial time-derivative, $\vec{h_c}$ is the angular momentum vector about the center of mass and $\vec{T_c}$ is the total external torque about the center of mass. Using the relation $\dot{\vec{\mathbf{r}}} = \mathring{\vec{\mathbf{r}}} + \vec{\omega} \times \vec{\mathbf{r}}$, where $\mathring{}$ is the mean time differentiation as seen in the spacecraft body frame F_b, we can rewrite the (2.19) as:

$$\mathring{\vec{\mathbf{h}}}_c + \vec{\omega}_b^n \times \vec{\mathbf{h}}_c = \vec{\mathbf{T}}_c \tag{2.20}$$

For a rigid body, the angular momentum vector expressed in $\mathcal{F}_b$ is given by:

$$\vec{\mathbf{h}}_c = \mathcal{F}_b^T I \omega_b^n \tag{2.21}$$

where I is the moment of inertia matrix about the center of mass expressed in body coordinates. Since F_b is embedded in the spacecraft, $\dot{\mathbf{I}} = 0$ From this, we have that in body coordinates

$$\mathring{\vec{\mathbf{h}}}_c = \mathcal{F}_b^T \mathbf{I} \dot{\omega}_b^n \tag{2.22}$$

so that in body coordinates the attitude dynamics become

$$\mathbf{I}\dot{\omega}_b^n + \omega_b^n \times (\mathbf{I}\omega_b^n) = \mathbf{T}_c \tag{2.23}$$

2.3 Inertia matrix

The inertia matrix of a spacecraft shall satisfy the following facts:

1. The inertia matrix is real, positive definire and symmetric, i.e. $\mathbf{I} = \mathbf{I}^T$ and $\mathbf{x}^T\mathbf{I}\mathbf{x} > 0$ for any non-zero vector $\mathbf{x} \neq 0$;

2. The inertia matrix is dependent on the orientation of F_b in the body. Let us consider two body frames F_{b_1} and F_{b_2}. Let $\mathbf{I_1}$ be the inertia matrix as computed in F_{b_1} and $\mathbf{I_2}$ be the inertia matrix as computed in F_{b_2}. Then $\mathbf{I_1}$ and $\mathbf{I_2}$ are related as follows:

$$\mathbf{I_2} = \mathbf{C}_{21}\mathbf{I_1}\mathbf{C}_{12} \tag{2.24}$$

where$\mathbf{C}_{21}$ is the rotation matrix representing the rotation from frame F_{b_1} to frame F_{b_2}.

3. It's always possible to find a body-fixed frame F_{b_p} such that the inertia matrix as computed in F_{b_p} is diagonal:

$$\mathbf{I}_p = \begin{bmatrix} I_x & 0 & 0 \\ 0 & I_y & 0 \\ 0 & 0 & I_z \end{bmatrix}$$

The frame F_{b_p} is called a principal axes frame. The attitude dynamics are simplified when expressed in this frame. Since $\mathbf{I}_p > 0$, it's clear that $I_x > 0$, $I_y > 0$ and $I_z > 0$. I_x I_y I_z are called the principal moments of inertia. The equations (2.23) becomes:

$$\begin{aligned} I_x\dot{\omega}_x + (I_z - I_y)\omega_y\omega_z &= T_x, \\ I_y\dot{\omega}_y + (I_x - I_z)\omega_x\omega_z &= T_y, \\ I_z\dot{\omega}_z + (I_y - I_x)\omega_x\omega_y &= T_z \end{aligned} \tag{2.25}$$

2.4 Environment

While describing the environment we'll do a distinction between the magnetic field model and the corresponding magnetic torque, which are used to control of the spacecraft attitude, and the disturbance torques.

2.4.1 Earth's magnetic field model

The analysis of the control torque required to control the spacecraft requires the knowledge of the Earth's magnetic field in the body coordinates as a function of the spacecraft position along the orbit. The magnetic field model used in this work is a simplified model of the magnetic field surrounding the Earth and it was assumed that the Earth's magnetic field can be expressed in terms of a magnetic dipole set along the geomagnetic axis, positive towards the geographic south pole. The dipole model of the Earth's magnetic field is a first order approximation of the rather complex true Earth's magnetic field. Due to effects of the interplanetary magnetic field, and the solar wind, the dipole model is particularly inaccurate at high L-shells (e.g., above L=3), but may be a good approximation for lower L-shells. For our purpose of a Lower Earth Orbit we can use the dipole approximation without loosing too much in accuracy.The following equations describe the dipole magnetic field [26]. First, define B_0 as the mean value of the magnetic field at the magnetic equator on the Earth's surface. Typically $B_0 = 3.12 \times 10^{-5} \quad [T]$. Then, the radial and azimuthal fields can be described as:

$$B_r = -2B_0 \left(\frac{R_E}{r}\right)^3 \cos\theta \tag{2.26}$$

$$B_\theta = -B_0 \left(\frac{R_E}{r}\right)^3 \sin\theta \tag{2.27}$$

$$|B| = B_0 \left(\frac{R_E}{r}\right)^3 \sqrt{1 + 3\cos^2\theta} \tag{2.28}$$

where R_E is the mean radius of the Earth (approximately 6371 km), r is the radial distance from the center of the Earth (using the same units as used for R_E), and θ is the azimuth measured from the north magnetic pole.

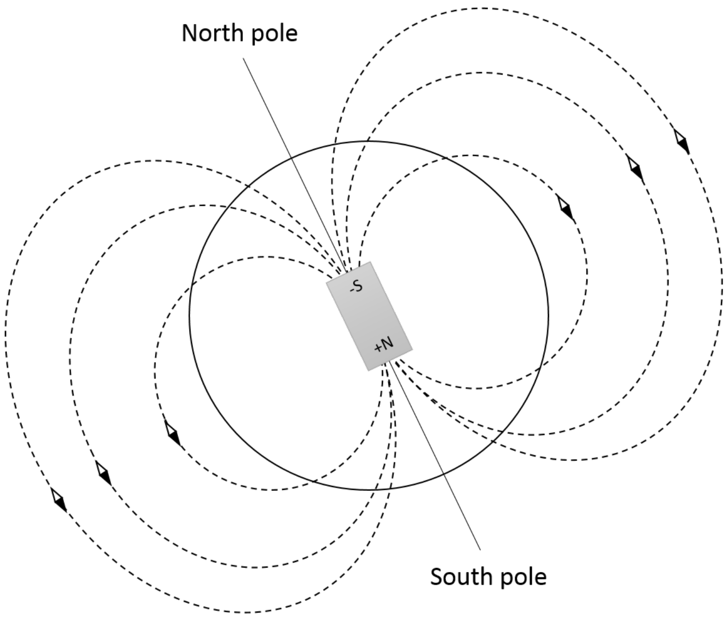

Figure 2.4: Dipole model of the Earth's magnetic field.

2.4.2 Disturbance torques

In this step, we determine the size of the external torques the ACS shall tolerate. Only three sources matter for a typical Earth-orbiting spacecraft, other than the magnetic-field torques, which here are used to control the spacecraft attitude. Disturbance can be affected by spacecraft orientation, design symmetry and mass properties. Typically, for a spacecraft in the low Earth orbit, the major disturbance torques are generated by:

- Solar radiation pressure,
- Aerodynamic drag,
- Gravity-gradient.

Solar radiation pressure

The photons from the sun can transfer on the spacecraft surfaces their momentum, with a magnitude near Earth of

$$p = 4.5 \times 10^{-6}\ N/m^2$$

There are different modes of interactions between the solar radiation and the spacecraft surface. We shall assume total absorption. From[8] we have that the total pressure torque is given by:

$$\overrightarrow{T}_s = \overrightarrow{c}_{ps} \times \overrightarrow{F}_s \tag{2.29}$$

where $\overrightarrow{c}_{ps}$ and $\overrightarrow{F}_s$ respectively are the center of solar pressure and the total force due to the solar pressure, defined as:

$$\overrightarrow{c}_{ps} = \frac{\int_S \overrightarrow{\rho}\,(\overrightarrow{n} \cdot \overrightarrow{s})\ dS}{\int_S (\overrightarrow{n} \cdot \overrightarrow{s})\ dS}$$

$$\overrightarrow{F}_s = \int_S d\overrightarrow{F}_s = -p\overrightarrow{s} \int_S \overrightarrow{n} \cdot \overrightarrow{s}\ dS \tag{2.30}$$

and the vectors $\overrightarrow{n}$, $\overrightarrow{s}$ and $\overrightarrow{p}$ are shown in Figure 2.5

Aerodynamic drag

The residual atmosphere in low Earth orbits is the cause of some aerodynamic drag. However the density is so low that conventional fluid mechanics do not

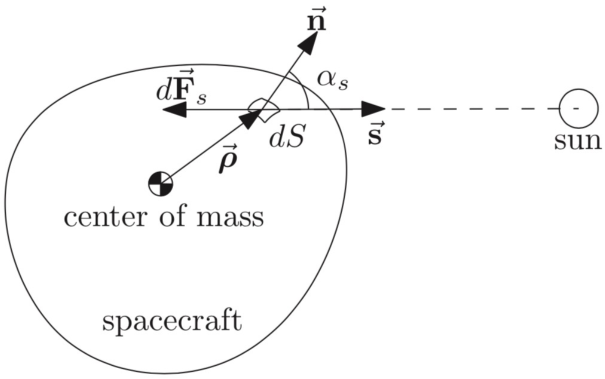

Figure 2.5: Solar radiation pressure on a surface element.

apply and the interaction between the atmosphere and the spacecraft must be treated at the molecular level. From [14] we have that:

$$\overrightarrow{T}_a = \mathbf{F}\left(C_{pa} - c_g\right) \tag{2.31}$$

where **F** is the aerodynamic drag:

$$\mathbf{F} = \frac{1}{2}\rho C_d A \mathbf{V}^2$$

while C_d represents the drag coefficient (usually between 2 and 2.5), ρ is the atmospheric density, A is the surface area and $\mathbf{V}$ is the spacecraft velocity vector. $c_{pa} - c_g$ represent the offset between the center of aerodynamic pressure and the center of gravity.

Gravity-gradient

The gravity-gradient torque is due to the fact that the Earth's gravitational force is not constant in space but decreases quadratically with the distance from the Earth's center. From [27] the gravitational force d**F** acting on a spacecraft mass element dm located at a position **r** from the geocenter is:

$$d\mathbf{F} = -\frac{\mu \mathbf{r}\, dm}{r^3} \tag{2.32}$$

where μ is the Earth's gravitational constant. Nonetheless, due to the symmetry on a 1U CubeSat, this disturbance torque is infinitesimal.

Furthermore, from subsequent analysis, it's clear that the only disturbance torques (although small compared to the actual control torques) that's worth considering is the aerodynamic torque since also the solar radiation pressure is small compared to the aerodynamic drag.

Chapter 3

Control Strategies

In this chapter we will discuss the stabilization techniques that will guarantee the spacecraft to be spin stabilized and how to control the spin axis direction. This will include both passive spin stabilization techniques, based on the design of the inertia matrix, and active control, both to active spin the satellite along one direction and control the spin axis orientation with respect to the external magnetic field.

3.1 Passive stabilization

Before thinking about the active spinning maneuvers we need to be sure that, even when the ACS will be shut off, the satellite will still have a stable spinning motion around the spinning axis. This will also help in the momentum damping process and in the spin axis precession control, as well as in the stability proof as it will guarantee to identify an equilibrium condition. Passive stabilization involves putting the spacecraft into a condition of naturally stable equilibrium. Spin stabilization is one of the oldest as well as simple form of passive stabilization, and it's used when the orientation about the direction of the spin axis is irrelevant. This condition, as we will see, is achieved by the design of the Inertia matrix. To evaluate the stability of spin equilibrium conditions lets consider a torque-free motion as in [8]. Since only spins around principal axes of inertia are equilibrium points, we consider only the following:

$$
\begin{aligned}
I_x\dot{\omega}_x + (I_z - I_y)\omega_y\omega_z &= 0 \\
I_y\dot{\omega}_y + (I_x - I_z)\omega_x\omega_z &= 0 \\
I_z\dot{\omega}_z + (I_y - I_x)\omega_x\omega_y &= 0
\end{aligned}
$$

and if the spinning axis is the z axis we will have:

$$\omega_x(t) = \omega_y(t) = 0, \quad \omega_z = \nu$$

that leads to:

$$\begin{aligned} I_x\dot{\omega}_x &= 0 \\ I_y\dot{\omega}_y &= 0 \\ I_z\dot{\omega}_z &= 0 \end{aligned}$$

This means that spinning around the z-axis is an equilibrium condition. Adding a perturbation ($\boldsymbol{\epsilon} = \epsilon_x, \epsilon_y \epsilon_z$) to the equilibrium condition we'll have, neglecting higher order terms:

$$\begin{aligned} I_x\dot{\epsilon}_x + (I_z - I_y)\nu\epsilon_y &= 0 \\ I_y\dot{\epsilon}_y + (I_x - I_z)\nu\epsilon_x &= 0 \\ I_z\dot{\epsilon}_z &= 0 \end{aligned}$$

which means that $\epsilon_z = \textit{constant}$ is a stable condition. If we now solve for ϵ_x and ϵ_y we'll find that both the equations in the frequency domain (applying the Laplace transform) will have the same poles as in [8]:

$$\hat{\epsilon_{x,y}}(s) = \frac{s\epsilon_{x,y}(0) - \dfrac{(I_{z,x} - I_{y,z})\nu}{I_{x,y}}\epsilon_{y,x}(0)}{s^2 + \alpha} \tag{3.1}$$

where α is:

$$\alpha = \frac{(I_z - I_y)(I_z - I_x)\nu^2}{I_x I_y}$$

and the only stable condition ($\alpha > 0$) leads to:

$$I_z > I_y \quad \text{and} \quad I_z > I_x$$

or

$$I_z < I_y \quad \text{and} \quad I_z < I_x$$

which means that, in a torque-free motion the stability condition is achieved while spinning around the major or minimum axis of inertia. Including the energy sink hypothesis (since in practice the motion is not torque free but the satellite will always be subject to energy dissipation) we'll get to the *Major Axis*

Rule which states that only spins around the major axis are asymptotically stable since:

$$T_{maj} < T_{min}$$

which means that the kinetic energy (T) is minimized for a major axis spin. The discovery of the major axis rule came after that the Explorer 1, axisymmetric and spin-stabilized about the minor axis of inertia, began to tumble after the deployment becoming unstable. With this in mind we have accurately controlled the mass distribution of the CubeSat to ensure that the major principal axis of inertia is the closest possible to the body z axis as that will be the desired spinning direction. After four design iterations with the team members and checking the mass distribution through Solidworks, we reached the following inertia matrix (in body coordinates):

$$\mathbf{J}_b = \begin{bmatrix} 1966658.25452 & -78777.90215 & 16304.64497 \\ -78777.90215 & 1980040.27412 & -11821.52277 \\ 16304.64497 & -11821.52277 & 2099362.78410 \end{bmatrix} \tag{3.2}$$

expressed in $g \times mm^2$. In principal axes of inertia the (3.2) becomes:

$$\mathbf{I}_b = \begin{bmatrix} 1892354.22649 & 0 & 0 \\ 0 & 2052301.82009 & 0 \\ 0 & 0 & 2101405.26616 \end{bmatrix} \tag{3.3}$$

where:

$$I_x = (0.73395, -0.67236, 0.09620)$$
$$I_y = (0.67140, 0.73961, 0.04683)$$
$$I_z = (-0.10264, 0.03022, 0.99426)$$

are the principal axes of inertia unity vectors taken at the center of mass. As we can see, the major principal axis of inertia (I_z) is close to the body z axis. This allow us to spin the satellite around the axis of maximum inertia while being close to the body z-axis from where the sail is going to be deployed.

3.2 Active spin axis control

When passive stabilization is established, we'll consider active spin axis control techniques using magnetorquers. Since the requirements are spinning the satellite around its principal axis of inertia and control the spinning axis direction to be parallel to the Earth's magnetic field lines we want to achieve these two conditions with two different maneuvers rather than achieving all at once. Also, we shall consider that the initial conditions after the deploying will be unknown and the satellite could be in a state of uncontrollable spin at unknown speed rate. Two algorithms have been studied for active spin rate control and one simple linear algorithm will be used to align the spin axis with the external magnetic field lines. First of all we need to ensure that the satellite reaches a controllable state and then we can actively drive the angular velocity vector to the desired state. This is typically done by detumbling. -Bdot algorithm is the most common way to detumble a satellite with initial unknown angular velocity. However, this may seem illogical to apply for a spinning satellite, since we don't want to completely get rid of the angular velocity along the spin axis direction. For this reason the two different algorithms for momentum damping that have been studied allow the spacecraft to reduce to zero the angular velocity components perpendicular to the spin axis only. Furthermore with those algorithms we don't need an initial detumbling since they work with any initial conditions. In both cases the spacecraft is allowed to spin around the spin axis regardless of the direction but only depending on the initial conditions. The torque produced by a magnetorquer placed in an external magnetic field (as the Earth's magnetic field) is given by the vector product of the torquer magnetic moment vector $\vec{\mathbf{m}}$ and the external magnetic field vector $\vec{\mathbf{B}}$ i.e.:

$$\vec{\mathbf{T}} = \vec{\mathbf{m}} \times \vec{\mathbf{B}} \tag{3.4}$$

It can be seen from (3.4) that the produced torque is always perpendicular to the instantaneous Earth's magnetic field vector. For this reason it's impossible to apply a full three-axis control, as well as apply a torque around an arbitrary axis using magnetorquers alone. For this reason the magnetic control seems to be underactuated. However, due to the variation of the magnetic field along the orbit, a full three-axis attitude control can be realized on average. This is true for orbits with significant inclination, since there's not much variation in the Earth's magnetic field for orbits near the equatorial plane, in particular

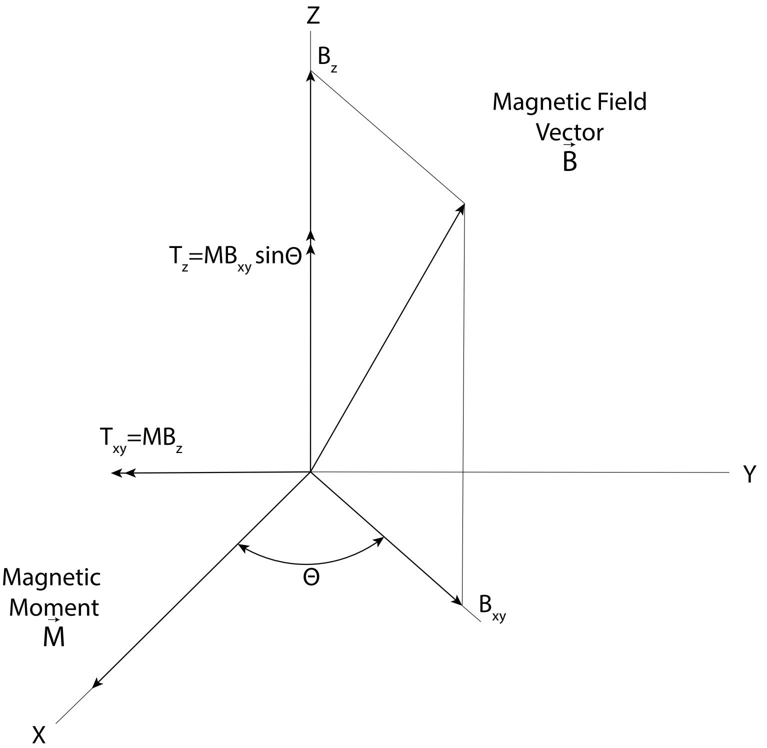

Figure 3.1: Torque due to a magnetic moment perpendicular to the spin axis.

since we consider a dipole model for the Earth's magnetic field. Furthermore, due to the weakness of the Earth's magnetic field, only coarse attitude control can be achieved with magnetorquers since the magnitude of the torque that can be generated is very small. Also, when using magnetorquers for attitude control, it's important not to actuate them while using the three-axis magnetometer are being sampled or evaluate and filter the disturbance generated by the magnetorquers. In our case it's been noticed that the disturbance in the magnetic field is very small and vanishes in a distance shorter than the distance between the magnetorquers and the magnetometer. For a spinning satellite, a magnetic moment applied in the spin axis direction produces a torque perpendicular to both the spin axis and the external field vector. This torque has no effect on the spin axis rate but will cause the direction of the spin axis to change, without altering it's spin magnitude. To produce a torque parallel or antiparallel to the spin axis, for spin rate control, requires a magnetic moment normal to the spin axis as we can see in Figure 3.1. In general magnetic control systems can be used for maneuvers for virtually all orbits with an altitude less than synchronous. For practical applications, it works best in LEO orbits (between 200 km to 2000 km of altitude, that is the first van Allen radiation belt limit) where we can take advantage of a stronger Earth's magnetic field. Magnetorquers typically can be permanent, "air"-core or iron core. Permament magnets are the heaviest type and are usually used for limited stabilization applications. The other two types are used for both stabilization and maneuvering. The magnetic dipole generated by a magnetorquer can be evaluated, in first approximation, as [12]:

$$m = niA \tag{3.5}$$

where:

- n is the winding count of the coil
- i is the applied current
- A is the coil area.

For a spin-stabilized spacecraft, magnetorquers can be mounted either around or perpendicular to the spin axis. Spin axis magnetic torquers can be used for reorientation, because torque cannot be applied along the spin axis, whereas a magnetorquer with its dipole in the spin plane can provide both angular velocity reorientation and spin rate control [27].

Chapter 4

Control Design

In this section we'll introduce the algorithms used to actively control the attitude of the spacecraft. Considering the limited space in the 1U Alpha CubeSat left available for avionics, a design choice has been made to use only magnetorquers for active attitude control while external measurements are done through a magnetometer and a gyroscope. As mentioned before for simplicity we'll divide the satellite motion into two stages for controlling the spinning rate and direction of the spacecraft. This allow us to make different assumptions on the spacecraft motion and behavior for each control law.

4.1 Nutation damping

The first stage correspond to the fast rotation of the satellite and we want to implement an algorithm that damps the transverse angular velocity and spins the satellite about its major principal axis of inertia . We have analyzed two different algorithms to achieve this goal and each of them have its advantages and disadvantages.

4.1.1 B-dot like Damper

This first algorithm is developed with similar assumptions made for the B-dot algorithm [17] but, instead of completely damping the momentum about all the three principal axes (and so the angular velocity), we only reduce the momentum to the desired magnitude (and direction in body axes). Assuming that the initial momentum difference (E) between the desired momentum (H_d)

and the current momentum (H) is expressed as:

$$E = \Delta H = H_d - H = \mathbf{I}\left(\boldsymbol{\omega}_d - \boldsymbol{\omega}\right) \tag{4.1}$$

where $\mathbf{I}$ is the inertia matrix and $\boldsymbol{\omega}_d$ is defined as:

$$\boldsymbol{\omega}_d = sign(\omega_z) \cdot \Omega \begin{bmatrix} 0 \\ 0 \\ 1 \end{bmatrix} \tag{4.2}$$

where $sign(\omega_z)$ is used because we want the spacecraft to spin around its principal axis of inertia with a spin magnitude equal to the scalar Ω, regardless of the sign i.e. if the satellite has an initial negative ω_z it will stay negative, otherwise it will stay positive. The goal of this control is to minimize the angular momentum difference. We implement a b-dot like algorithm for the magnetic dipole, as follows:

$$\mathbf{m} = -\frac{k}{\parallel B \parallel^2} \boldsymbol{\Delta\omega} \times \mathbf{B} \tag{4.3}$$

The gain of (4.3) is calculated as [4]:

$$k = \frac{4\pi}{T_{orb}} \left(1 + \sin \xi_m\right) J_{min} \tag{4.4}$$

where T_{orb} is the orbital period in seconds, ξ_m is the inclination of the spacecraft orbit relative to the geomagnetic equatorial plane and J_{min} is the minimum principal moment of inertia.

4.1.2 Kane Damper

This control algorithm uses what's called the Kane Damper. This name derives from Thomas R. Kane, which studied the effects of energy dissipation on a spinning spacecraft as in [5]. In the present work, instead of only tanking into account the energy dissipation effects, those are used to produce a torque that will drive the spacecraft's angular momentum vector to be parallel to the maximum principal axis of inertia. Hence we will use the same model used from Kane in [5], described as follows. The Kane Damper is a *fictional* device that models the interaction between a spherical damper and the spacecraft. Lets suppose to have inside the spacecraft a spherical cavity, inside of witch there is another smaller spherical rigid body. In the gap between the two bodies there is a (fictional) viscous fluid as shown in Figure 4.1

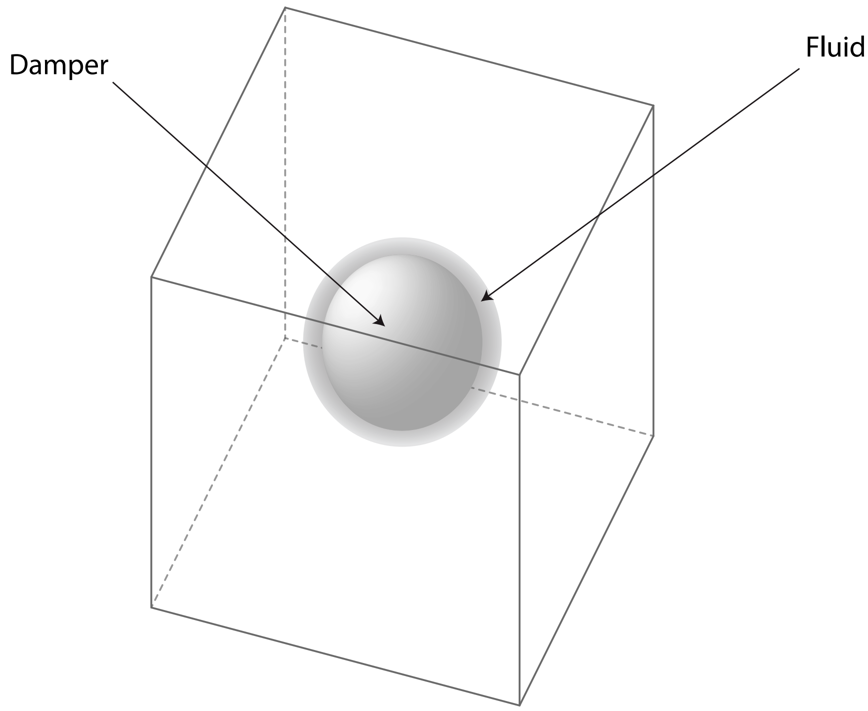

Figure 4.1: Kane Damper model.

In this situation the total angular momentum is given by:

$$\mathbf{H} = \mathbf{I}_d \boldsymbol{\omega}_n^d + \mathbf{I}_b \boldsymbol{\omega}_n^b \tag{4.5}$$

where $\mathbf{I}_d$ and $\mathbf{I}_b$ represent the inertia matrices of the damper and the external body respectively and the notation $\boldsymbol{\omega}_n^d$ means the angular velocity of the damper with respect to the inertial frame. Without external perturbations, this system is in equilibrium thus:

$$\begin{aligned} \left.\frac{\partial \mathbf{H}}{\partial t}\right|_n &= 0 \\ &= \left(\mathbf{I}_d \dot{\boldsymbol{\omega}}_n^d + \boldsymbol{\omega}_n^b \times \mathbf{I}_d \boldsymbol{\omega}_n^d\right) + \left(\mathbf{I}_b \dot{\boldsymbol{\omega}}_n^b + \boldsymbol{\omega}_n^b \times \mathbf{I}_b \boldsymbol{\omega}_n^b\right) = 0 \end{aligned} \tag{4.6}$$

where $|_n$ means that the time derivative is calculated with respect to the inertial frame. We notice that the terms inside the latter parenthesis of the (4.6) are the dynamical equation of motion of a rotating rigid body (the spacecraft). Thus we may design a controller that acts like the aforementioned damper. We know that the fluid in the gap between the two bodies will tend to eliminate the difference between the two body's angular velocities as:

$$\boldsymbol{\tau}_d = c\left(\boldsymbol{\omega}_n^b - \boldsymbol{\omega}_n^d\right) \tag{4.7}$$

Now if we define:

$$\mathbf{I}_d\dot{\boldsymbol{\omega}}_n^d + \boldsymbol{\omega}_n^b \times \mathbf{I}_d\boldsymbol{\omega}_n^d = \boldsymbol{\tau}_d \tag{4.8}$$

we also have that

$$\mathbf{I}_b\dot{\boldsymbol{\omega}}_n^b + \boldsymbol{\omega}_n^b \times \mathbf{I}_b\boldsymbol{\omega}_n^b = -\boldsymbol{\tau}_d \tag{4.9}$$

the last one is the rotational equation of motion of a rigid body, where τ_d represent the external torques. Now we can introduce some assumptions:

- The central body (the damper) is modeled as a sphere. This allow us to define it's inertia matrix as:

  $$\mathbf{I}_d = I_d \cdot \begin{bmatrix} 1 & 0 & 0 \\ 0 & 1 & 0 \\ 0 & 0 & 1 \end{bmatrix} \tag{4.10}$$

  where I_d is a scalar;

- The angular velocity of the damper with respect to the inertial frame can be described as:

  $$\boldsymbol{\omega}_n^d = \boldsymbol{\omega}_b^d + \boldsymbol{\omega}_n^b \tag{4.11}$$

  as well as it's time derivative:

  $$\dot{\boldsymbol{\omega}}_n^d = \dot{\boldsymbol{\omega}}_b^d + \dot{\boldsymbol{\omega}}_n^b \tag{4.12}$$

Introducing (4.10) and (4.11) in (4.8) we have:

$$\begin{aligned} \boldsymbol{\tau}_d &= I_d\dot{\boldsymbol{\omega}}_n^d + I_d\boldsymbol{\omega}_n^b \times \boldsymbol{\omega}_n^d = \\ &= I_d\dot{\boldsymbol{\omega}}_n^d + I_d\boldsymbol{\omega}_n^b \times \left(\boldsymbol{\omega}_b^d + \boldsymbol{\omega}_n^b\right) = \\ &= I_d\left(\dot{\boldsymbol{\omega}}_n^d + \boldsymbol{\omega}_n^b \times \boldsymbol{\omega}_b^d\right) \end{aligned} \tag{4.13}$$

since $\boldsymbol{\omega}_n^b \times \boldsymbol{\omega}_n^b = 0$. Now introducing (4.7) and (4.12) we obtain:

$$c\left(\boldsymbol{\omega}_n^b - \boldsymbol{\omega}_n^d\right) = -c\,\boldsymbol{\omega}_b^d = I_d\left[\left(\dot{\boldsymbol{\omega}}_n^d + \dot{\boldsymbol{\omega}}_n^b\right) + \boldsymbol{\omega}_n^b \times \boldsymbol{\omega}_b^d\right] \tag{4.14}$$

from which we get:

$$\dot{\boldsymbol{\omega}}_b^d = -\dot{\boldsymbol{\omega}}_n^b - \frac{c}{I_d}\left(\underline{\mathbf{1}} + \boldsymbol{\omega}_n^{b\times}\right)\boldsymbol{\omega}_b^d \tag{4.15}$$

where $\underline{\mathbf{1}}$ is the 3×3 identity matrix and $\boldsymbol{\omega}_n^{b\times}$ is the skew anti-symmetric matrix defined as:

$$\boldsymbol{\omega}_n^{b\times} = \begin{bmatrix} 0 & -\omega_{n_3}^b & \omega_{n_2}^b \\ \\ \omega_{n_3}^b & 0 & -\omega_{n_1}^b \\ \\ -\omega_{n_2}^b & \omega_{n_1}^b & 0 \end{bmatrix}$$

The equation (4.15) is a system of first order differential equations in $\boldsymbol{\omega}_d^b$ that, along with (4.7) and (4.9) let us define the behavior of the spacecraft dynamics. The initial condition required to solve (4.15) are given by:

$$\boldsymbol{\omega}_b^d(t_0) = \frac{\left|H\right|}{I_d} \cdot \begin{bmatrix} 0 \\ 0 \\ 1 \end{bmatrix} \tag{4.16}$$

where $\left|H\right|$ is the required angular momentum. Furthermore, $\dot{\boldsymbol{\omega}}_n^b$ may come from accelerometer measurements or can be approximated by:

$$\dot{\boldsymbol{\omega}}_n^b \simeq \frac{\boldsymbol{\omega}_n^b(t_2) - \boldsymbol{\omega}_n^b(t_1)}{\Delta t} \tag{4.17}$$

Now, if we consider this controller applied to magnetic torquers, we must recall that, with a magnetic actuation, the final torque is given by:

$$\mathbf{T} = \mathbf{m} \times \mathbf{B} \tag{4.18}$$

where $\mathbf{m}$ is the external magnetic dipole generated by the magnetorquers and $\mathbf{B}$ is the external magnetic field in the body coordinate system. Hence we shall modify the (4.9) like:

$$\mathbf{I}_b \dot{\boldsymbol{\omega}}_n^b + \boldsymbol{\omega}_n^b \times \mathbf{I}_b \boldsymbol{\omega}_n^b = \mathbf{T} = \mathbf{m} \times \mathbf{B} \tag{4.19}$$

where:

$$m = -\frac{\boldsymbol{\tau}_d \times \mathbf{B}}{\parallel \mathbf{B} \parallel^2} \tag{4.20}$$

the cross product in $\mathbf{m}$ is to guarantee the orthogonality between $\mathbf{m}$ and $\mathbf{B}$. Finally (4.19) rewrites as:

$$\mathbf{I}_b \dot{\boldsymbol{\omega}}_n^b + \boldsymbol{\omega}_n^b \times \mathbf{I}_b \boldsymbol{\omega}_n^b = -\left(\boldsymbol{\tau}_d \times \mathbf{b}\right) \times \mathbf{b} \tag{4.21}$$

where $\mathbf{b} = \mathbf{B} / \parallel \mathbf{B} \parallel$.

4.1.3 Magnetic dipole and trade-off analysis

In both the cases of the B-dot like controller and the Kane Damper, the torque is proportional to some form of $\boldsymbol{\Delta\omega}$, where:

$$\boldsymbol{\tau} = -k\boldsymbol{\Delta\omega} = -k\left(\boldsymbol{\omega}_d - \boldsymbol{\omega}\right) \tag{4.22}$$

for the first momentum damper and:

$$\boldsymbol{\tau} = -c\boldsymbol{\Delta\omega} = -c\left(\boldsymbol{\omega}_n^b - \boldsymbol{\omega}_n^d\right) \tag{4.23}$$

for the Kane Damper. Also, in both cases the magnetic dipole is defined as:

$$\mathbf{m} = \frac{\boldsymbol{\tau} \times \mathbf{B}}{\|\mathbf{B}\|^2}$$

such that the applied torque from (4.18) becomes:

$$\mathbf{T} = \mathbf{m} \times \mathbf{B} = (\boldsymbol{\tau} \times \mathbf{b}) \times \mathbf{b} \tag{4.24}$$

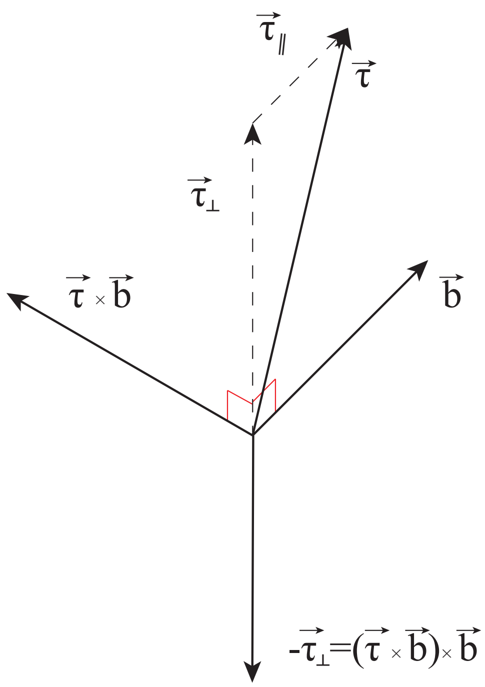

Figure 4.2: Double external product between $\boldsymbol{\tau}$ and the unit vector $\mathbf{b}$.

In this way, by multiplying twice $\boldsymbol{\tau}$ with the unit vector $\mathbf{b}$ we have that the applied torque becomes $-\boldsymbol{\tau}_{\perp}$, as seen in Figure 4.2, where $\boldsymbol{\tau}_{\perp}$ is the component of $\boldsymbol{\tau}$ perpendicular to the external magnetic field. This means that, to make the control law work with magnetic actuation we only need to multiply by -1 the proportional coefficient and then we will have, in general:

$$\mathbf{T} \leq -\boldsymbol{\tau} \tag{4.25}$$

which means that we'll have the maximum torque only if $\boldsymbol{\tau}$ and $\mathbf{B}$ are perpendicular. Furthermore, while considering the magnetic dipole as the external product of the control torque and the external magnetic field, we already get rid of the unnecessary component of the torque, parallel to $\mathbf{B}$, that won't be able to interact with the spacecraft.
To select one controller rather than the other, we've done some evaluation. Even though the first control law is simpler and reliable, it needs to know precisely the direction of the major principal axis of inertia since the $\boldsymbol{\Delta H}$, and thus $\boldsymbol{\Delta\omega}$ are defined in the principal directions. This can be achieved in the latest design phases of the spacecraft by effectively measuring the mass distribution (rather than rely on the CAD mass distribution, even if accurate) or by using some inertia matrix identification techniques [1], [19]. On the other and, the Kane Damper has an elevate computational cost since it requires to integrate the fictional damper dynamics but it doesn't need to know the direction of the axis of maximum inertia a priori since the model itself will lead the spacecraft to rotate about that axis provided that that axis actually exists and that it is clearly greater than the others (this means that it doesn't spare the effort in designing the mass distribution properly, in particular to make the major principal axis of inertia the closest possible to the pointing direction). Moreover, the increment in computational cost found in the Kane Damper is still less than that required by the inertia matrix identification. For this reason the second controller has been chosen for damping the transverse components of the angular velocity.

4.2 Spin axis pointing

Lets consider the spacecraft dynamics expressed in (2.23):

$$\mathbf{I}\dot{\boldsymbol{\omega}} + \boldsymbol{\omega} \times \mathbf{I}\boldsymbol{\omega} = \mathbf{T} \tag{2.23}$$

We can expand the previous equation along the three principal axis of inertia as seen in (2.26):

$$\begin{aligned} I_x\dot{\omega}_x + (I_z - I_y)\,\omega_y\omega_z &= T_x \\ I_y\dot{\omega}_y + (I_x - I_z)\,\omega_x\omega_z &= T_y \\ I_z\dot{\omega}_z + (I_y - I_x)\,\omega_x\omega_y &= T_z \end{aligned} \tag{4.26}$$

where ω_x, ω_y, ω_z are the angular velocities calculated in the body axes. For a satellite spinning around the maximum principal axis of inertia (stable) we can assume ω_x, $\omega_y \approx 0$ and $\omega_z = \omega_s$ constant. With this assumption, the dynamics equations can be reasonably simplified as:

$$\begin{aligned} I_x\dot{\omega}_x &= T_x \\ I_y\dot{\omega}_y &= T_y \\ I_z\dot{\omega}_z &= T_z \end{aligned} \tag{4.27}$$

or, in compact form:

$$\mathbf{I}\dot{\boldsymbol{\omega}} = \mathbf{T} \tag{4.28}$$

With the last equations the problem assumes a linear form (without the $\omega_i\omega_j$ product) and the precession controller can be modeled as a linear controller where the magnetic dipole can be expressed as:

$$\mathbf{m} = \frac{\mathbf{u}}{\parallel \mathbf{B}^b \parallel} \tag{4.29}$$

and the applied torque becomes:

$$T = \frac{\mathbf{u} \times \mathbf{B}}{\parallel \mathbf{B}^b \parallel} = \frac{S\,(\mathbf{u})\,\mathbf{B}^b}{\parallel \mathbf{B}^b \parallel} \tag{4.30}$$

where $S(\mathbf{u})$ is the anti-symmetric skew matrix defined as:

$$S(\mathbf{u}) = \begin{bmatrix} 0 & -u_z & u_y \\ u_z & 0 & -u_x \\ -u_y & u_x & 0 \end{bmatrix} \tag{4.31}$$

The control input $\mathbf{u}$ may be expressed with a PD controller:

$$\mathbf{u} = K_p\mathbf{e} + K_d\dot{\mathbf{e}} \tag{4.32}$$

where $\mathbf{e}(t)$ is the local relative attitude error. Since our goal is to align the spin axis with the external magnetic field, $\mathbf{e}(t)$ is defined as:

$$e = \sin^{-1}\theta_{e_zB} = \sin^{-1}\left(\frac{\hat{\mathbf{e_z}} \times \mathbf{B}}{|\mathbf{e_z}||\mathbf{B}|}\right) = \sin^{-1}\left(\hat{\mathbf{e_z}} \times \mathbf{b}\right) \tag{4.33}$$

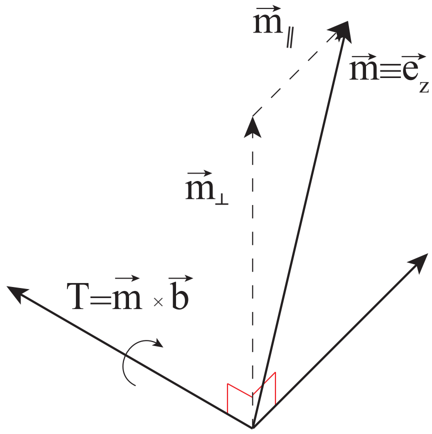

Figure 4.3: Torque produced by a magnetic dipole in the e_z direction.

where $\hat{\mathbf{e_z}}$ is the unity vector representing the axis of symmetry, assumed to be very close to the maximum principal axis of inertia, and $\mathbf{b} = \mathbf{B}/ \parallel \mathbf{B} \parallel$. The last assumption leads us to implement a magnetic dipole along the spacecraft z-axis. As seen in Section 3.2, applying a magnetic dipole along the spin axis we'll produce a torque perpendicular to both the spin axis and the external magnetic field vector as in Figure 4.3. Due to the variation of the Earth's magnetic field along the orbit position, this torque has no effect on the spin rate and will tend to precess the spin axis around the magnetic field lines and slowly will make the spin axis parallel to the Earth's magnetic field. For this reason for this stage, the magnetic dipole will be generated using only the magnetorquer parallel to the spin axis, i.e.

$$m = \begin{bmatrix} 0 \\ 0 \\ m_z \end{bmatrix} \tag{4.34}$$

Also, since the detumbling stage will let the spacecraft spin around its major principal axis of inertia regardless of the direction (clockwise or counterclockwise, depending on the initial conditions), we also need this control law to align the two axes following the shortest path, i.e. the spacecraft's spin axis final alignment will be of $n\,\pi$ degrees with respect to the external magnetic field, with n = 0,1. For this reason, we'll also analyze the cosine of the angle between the z-axis and the magnetic field:

$$\cos\theta_{\omega B} = \frac{\boldsymbol{\omega} \cdot \mathbf{B}}{|\boldsymbol{\omega}||\mathbf{B}|} \tag{4.35}$$

and then we apply the sign function:

$$sign(x) = \begin{cases} -1 & \text{if} \quad x < 0 \\ 0 & \text{if} \quad x = 0 \\ 1 & \text{if} \quad x > 0 \end{cases} \tag{4.36}$$

to the cosine of the angle $\theta_{\omega B}$ and to the quantity ω_z that represent the spin rate. Using together (4.29) and (4.32) to (4.36) we obtain the magnetic dipole as:

$$\mathbf{m} = \frac{\left(\sin^{-1}\left(\frac{\hat{\mathbf{e}}_z \times \mathbf{B}}{|\mathbf{B}|}\right) K_p + \frac{\partial}{\partial t}\sin^{-1}\left(\frac{\hat{\mathbf{e}}_z \times \mathbf{B}}{|\mathbf{B}|}\right) K_d\right)}{|\mathbf{B}|} K \begin{bmatrix} 0 \\ 0 \\ 1 \end{bmatrix} \tag{4.37}$$

where K represents:

$$K = sign\left(\cos\left(\theta_{\omega B}\right)\right) \cdot sign\left(\cos\left(\omega_z\right)\right)$$

and allows to align the spin axis to the external magnetic field regardless of the spin rate sign and initial conditions.

Chapter 5

Stability analysis and gain selection

Given a control system, the first and most important question about its various properties is whether it is stable or not, since an unstable control system can be potentially dangerous. For this reason stability theory plays a central role in systems engineering. Thus, before getting the gains for the previous control algorithms, we need to perform a stability analysis first. That has been done for both the nonlinear and linear controller. In particular, for the nonlinear controller we first assessed the asymptotic stability in the sense of Lyapunov. Then we linearized the control law around the equilibrium points and we assessed the linear stability as well. For the linear pointing controller we only used linear techniques to ensure asymptotic stability and then we evaluate the time and frequency response for gain selection. We'll now introduce the Lyapunov's Direct Method for general non linear stability proof. For linear asymptotic stability we'll study the position of the transfer function's poles in the complex plane.

5.1 Lyapunov's Direct Method

Lyapunov stability theory is a standard tool and one of the most important tools in the analysis of nonlinear systems [2], [8], [13]. It is typically used to study the stability of equilibrium points. An equilibrium point is *stable* if all solutions starting nearby stay nearby, it is *asymptotically stable* if all solutions starting nearby stay nearby and also tend to the equilibrium point itself as time approaches to infinity. Otherwise it is *unstable*. If we consider the autonomous system:

$$\dot{x} = f(x) \tag{5.1}$$

where $f : D \to R^n$ is some open set containing the origin. Suppose $\overline{x} \in D$ is an equilibrium point of (5.1), i.e. $f(\overline{x}) = 0$. For convenience we suppose that $\overline{x} = 0$ since, for every $\overline{x} \neq 0$ we can apply a change of variable $y = x - \overline{x}$. We can state that an equilibrium point $x = 0$ is:

- *Stable* if, for each $\varepsilon > 0$, there is $\delta = \delta(\varepsilon) > 0$ such that

$$\parallel x(0) \parallel < \delta \Rightarrow \parallel x(t) \parallel < \varepsilon, \quad \forall t \geq 0$$

- *Unstable* if it is not stable.

- *Asymptotically stable* if it is stable and δ can be chosen such that

$$\parallel x(0) \parallel < \delta \Rightarrow \lim_{t \to \infty} x(t) = 0$$

This can also proved by considering a continuously differentiable scalar function $V(x) : D \to R$, such that $V(\mathbf{0}) = 0$ and $V(\mathbf{x}) > 0$ for $\mathbf{x} \in D$ with $\mathbf{x} \neq \mathbf{0}$. Suppose that along solutions $\mathbf{x}(t) \in D$

$$\dot{V}(\mathbf{x}) \leq 0 \tag{5.2}$$

Then, $\mathbf{x} = \mathbf{0}$ is stable. Furthermore if

$$\dot{V}(\mathbf{x}) < 0 \quad \text{for} \quad \mathbf{x} \neq \mathbf{0} \tag{5.3}$$

then $\mathbf{x} = \mathbf{0}$ is asymptotically stable. The function $V(\mathbf{x})$ is called *Lyapunov function candidate* and, if stability is proven, *Lyapunov function.* We can note that $V(\mathbf{x})$ is the time derivative of $V(\mathbf{x})$ along the solution trajectory and can be found by the chain rule:

$$\dot{V}(\mathbf{x}) = \frac{\dot{V}(\mathbf{x})}{dt} = \frac{\partial V}{\partial x}\dot{\mathbf{x}} = \frac{\partial V}{\partial x} f(\mathbf{x}) \tag{5.4}$$

This establishes the local stability. To include global stability, $v(\mathbf{x})$ shall have the property that

$$\parallel \mathbf{x} \parallel \to \infty \quad \text{implies that} \quad V(\mathbf{x}) \to \infty \tag{5.5}$$

then $\mathbf{x} = \mathbf{0}$ is globally asymptotically stable.
For a linear time-invariant system in the form of:

$$\dot{\mathbf{x}} = A\mathbf{x} \tag{5.6}$$

an equilibrium point $\mathbf{x} = 0$ is *stable* if and only if all eigenvalues of A satisfy $Re(\Gamma_i) \leq 0$ and for every eigenvalue with $Re(\Gamma_i) = 0$ end multiplicity $q_i \geq 2$, $rank(A - \Gamma_i I) = n - q_i$, where n is the dimension of $\mathbf{x}$. If all the eigenvalues of A have negative real part, the equilibrium point is *asymptotically stable*.

5.2 Stability proof

5.2.1 B-dot like Damper

Lets recall the momentum difference between the desired and current angular momentum:

$$E = \Delta H = H_d - H = \mathbf{I}\left(\boldsymbol{\omega}_d - \boldsymbol{\omega}\right) \tag{4.1}$$

As in [22], [24] we start considering the equation of rigid body dynamics:

$$\frac{dH}{dt} = T + D \tag{5.7}$$

where T is the external torque and D is the sum of external disturbances. Substituting in the previous (4.1) we obtain the as Lyapunov function candidate:

$$V = \frac{dE}{dt} = -T - D \tag{5.8}$$

noticing that $dH_d/dt = 0$. Lets now consider the time derivative of the square momentum error, thus we have:

$$\dot{V} = \frac{dE^2}{dt} = 2E\frac{dE}{dt} = -2\Delta H \cdot T - 2\Delta H \cdot D \tag{5.9}$$

The sufficient asymptotic stability condition for E is $\frac{dE^2}{dt} < 0$. Substituting (4.3) in

$$\mathbf{T} = \mathbf{m} \times \mathbf{B} \tag{5.10}$$

we have:

$$T = -k\left(\boldsymbol{\Delta\omega} \times \mathbf{b}\right) \times \mathbf{b} = k\left(I_3 - \mathbf{b}\mathbf{b}^T\right)\boldsymbol{\Delta\omega} \tag{5.11}$$

where $\mathbf{b} = \mathbf{B}/\parallel \mathbf{B} \parallel$ and I_3 is the 3×3 identity matrix. Substituting (5.11) in (5.9), neglecting the disturbance torques assuming them to be negligibly small compared to T, and using (4.1) we have:

$$\dot{V} = \frac{dE^2}{dt} = -2k\mathbf{I}\boldsymbol{\Delta\omega}^T\left(I_3 - \mathbf{b}\mathbf{b}^T\right)\boldsymbol{\Delta\omega} \tag{5.12}$$

Since the eigenvalues of $\left(I_3 - \mathbf{b}\mathbf{b}^T\right)$ are always 0, 1, and 1, then (5.12) is only negative semi-definite i.e. (5.12) is zero only when $\boldsymbol{\Delta\omega}$ is zero or when it is parallel to b i. e. at the equilibrium point. The gain k of (4.3) could be selected as showed in Chapter 4 but, as stated in the same chapter, we have decided to use the Kane Damper for spinning the satellite around the major principal axes of inertia.

5.2.2 Kane Damper

For the Kane Damper we can select, as a Lyapunov function candidate, an energy function. In particular we can use the total kinetic energy:

$$V = \mathbf{T} = \frac{1}{2}\boldsymbol{\omega}_n^{b^T}\mathbf{I}_b\boldsymbol{\omega}_n^b + \frac{1}{2}\boldsymbol{\omega}_n^{d^T}\mathbf{I}_b\boldsymbol{\omega}_n^d \tag{5.13}$$

where the first term is relative to the body (spacecraft) and the second to the fictional damper. We define the equilibrium point as:

$$\boldsymbol{\omega}_0 = \boldsymbol{\omega}_{n_{eq}}^b = \boldsymbol{\omega}_{n_{eq}}^d = \Omega \cdot \begin{bmatrix} 0 \\ 0 \\ 1 \end{bmatrix} \tag{5.14}$$

We notice that at the equilibrium point, with a change of coordinates:

$$\begin{aligned} \boldsymbol{\omega}_{n_0}^b &= \boldsymbol{\omega}_n^b - \boldsymbol{\omega}_0 \\ \boldsymbol{\omega}_{n_0}^d &= \boldsymbol{\omega}_n^d - \boldsymbol{\omega}_0 \end{aligned}$$

we have $V(\mathbf{x}) = 0$, where the vector $\mathbf{x}$ is represented by:

$$\mathbf{x} = \begin{bmatrix} \boldsymbol{\omega}_n^b \\ \boldsymbol{\omega}_n^d \end{bmatrix} \tag{5.15}$$

By applying the time derivative to the Lyapunov function candidate we obtain:

$$\dot{V} = \dot{\mathbf{T}} = \boldsymbol{\omega}_n^{b^T}\mathbf{I}_b\dot{\boldsymbol{\omega}}_n^b + \boldsymbol{\omega}_n^{d^T}\mathbf{I}_b\dot{\boldsymbol{\omega}}_n^d \tag{5.16}$$

Substituting the time derivative terms in (5.16) with the dynamic equations of the body and damper:

$$\mathbf{I}_b\dot{\boldsymbol{\omega}}_n^b + \boldsymbol{\omega}_n^b \times \mathbf{I}_b\boldsymbol{\omega}_n^b = -\boldsymbol{\tau}_d \tag{4.9}$$

$$\mathbf{I}_d\dot{\boldsymbol{\omega}}_n^d + \boldsymbol{\omega}_n^b \times \mathbf{I}_d\boldsymbol{\omega}_n^d = \boldsymbol{\tau}_d \tag{4.8}$$

we obtain:

$$\dot{V} = \boldsymbol{\omega}_n^{b^T}\mathbf{I}_b\mathbf{I}_b^{-1}\left[-\boldsymbol{\tau}_d - \boldsymbol{\omega}_n^b \times \mathbf{I}_b\boldsymbol{\omega}_n^b\right] + \boldsymbol{\omega}_n^{d^T}\mathbf{I}_b\mathbf{I}_d^{-1}\left[\boldsymbol{\tau}_d - \boldsymbol{\omega}_n^b \times \mathbf{I}_d\omega_n^d\right] \tag{5.17}$$

which we can rearrange as:

$$\dot{V} = -\boldsymbol{\omega}_n^{b^T}\boldsymbol{\tau}_d + \boldsymbol{\omega}_n^{d^T}\boldsymbol{\tau}_d - \left[-\boldsymbol{\omega}_n^{b^T}\left(\boldsymbol{\omega}_n^b \times \mathbf{I}_b\boldsymbol{\omega}_n^b\right) + \boldsymbol{\omega}_n^{d^T}\left(\boldsymbol{\omega}_n^b \times \mathbf{I}_d\boldsymbol{\omega}_n^d\right)\right] \tag{5.18}$$

The terms inside the square brackets is equal to zero thanks to the property of the triple product, i.e.

$$a \cdot (b \times c) = b \cdot (c \times a) = c \cdot (a \times b)$$

In fact:

$$\begin{aligned}\boldsymbol{\omega}_n^{b^T}\left(\boldsymbol{\omega}_n^b \times \mathbf{I}_b\boldsymbol{\omega}_n^b\right) &= \mathbf{I}_b\boldsymbol{\omega}_n^b\left(\boldsymbol{\omega}_n^b \times \boldsymbol{\omega}_n^b\right) = 0 \\ \boldsymbol{\omega}_n^{d^T}\left(\boldsymbol{\omega}_n^b \times \mathbf{I}_d\boldsymbol{\omega}_n^d\right) &= \boldsymbol{\omega}_n^b\left(\mathbf{I}_d\boldsymbol{\omega}_n^d \times \boldsymbol{\omega}_n^d\right) = 0\end{aligned}$$

The first one is zero for obvious reasons, while the second is zero only thanks to the property of the fictional damper inertia matrix $\mathbf{I}_d$ as seen in Chapter 4. Rewriting (5.18) we have:

$$\dot{V} = -\boldsymbol{\omega}_n^{b^T}\boldsymbol{\tau}_d + \boldsymbol{\omega}_n^{d^T}\boldsymbol{\tau}_d = \left(\boldsymbol{\omega}_n^d - \boldsymbol{\omega}_n^b\right)^T\boldsymbol{\tau}_d \tag{5.19}$$

recalling the definition of $\boldsymbol{\tau}_d$:

$$\boldsymbol{\tau}_d = c\left(\boldsymbol{\omega}_n^b - \boldsymbol{\omega}_n^d\right) \tag{4.7}$$

we finally have:

$$\dot{V} = \underbrace{\left(\boldsymbol{\omega}_n^d - \boldsymbol{\omega}_n^b\right)^T}_{k^T} c \underbrace{\left(\boldsymbol{\omega}_n^b - \boldsymbol{\omega}_n^d\right)}_{-k} = -ck^2 \tag{5.20}$$

As we can see, in general, the Kane Damper is asymptotically stable for any positive c at equilibrium points having either positive or negative Ω in (5.14). If we now consider the magnetic actuation, as seen in (4.24) and (4.25) we only need to cross multiply twice the control torque with $b = \mathbf{B}/|\mathbf{B}|$ and this will lead to a change in sign but will have no effect on stability since the actual torque will never be greater than the control torque. Moreover, the only change we shall introduce is on the sign of (4.7), that means that the Kane Damper is stable for any negative values of c or, as we did, changing the sign of the control torque a priori. The goal now is to select the proper values for I_d and c. As we seen the controller is stable for any value of c as well as I_d, thus our choice is based on time performance, while operating a simulation-based optimization [9].

Simulation-based optimization for gain selection.

The simulation-based optimization integrates optimization techniques into simulation analysis. Because of the complexity of the simulation, this is a time-consuming method and improves the performance partially. To obtain the optimal solution with minimum computation and time, the problem is solved iteratively where in each iteration the solution moves closer to the optimum solution. Such methods are known as 'numerical optimization' or 'simulation-based optimization [18]. With a good mathematical model such as before, computer-based simulations can give useful information about its behavior. The goal is to evaluate the effect of different values of I_d and c on the system and find the optimal values in terms of time response. Moreover, the simulations are limited by the on-board processor performances. One way could be running simulation experiments for all possible input variables.

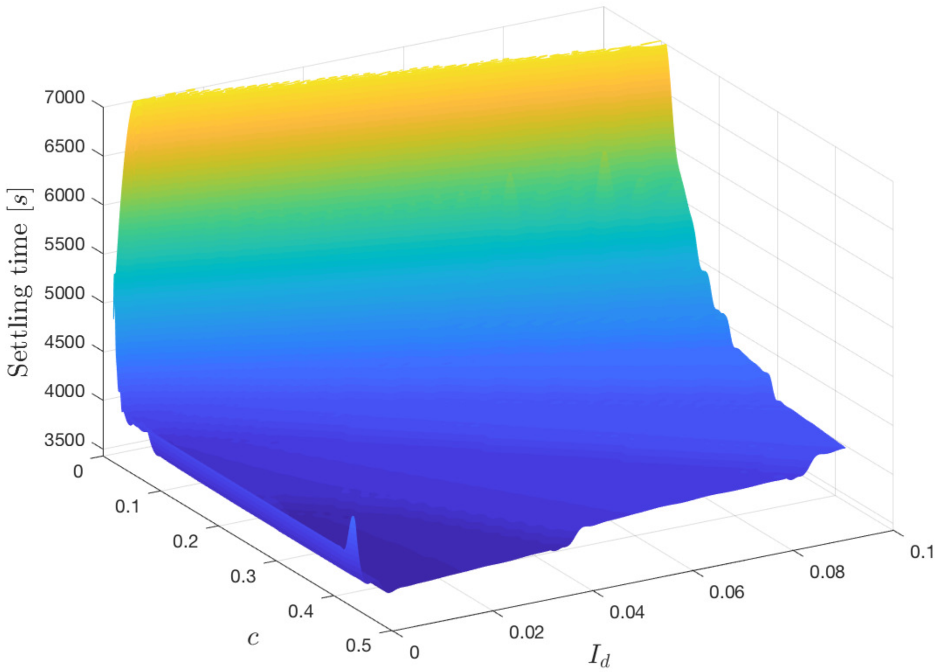

Figure 5.1: Simulation-based settling time varying I_d and c.

In Figure 5.1 are plotted the settling times of ~ 4500 simulations while varying both I_d and c values. The c value is limited by the on-board processor performance (in the design process we decided not to operate at a frequency higher than 100 Hz). In this analysis we found that the minimum settling time, and the corresponding I_d and c, is:

Settling Time	3448.5 $[s]$
I_d	0.0082551
c	0.41837

Table 5.1: Best values of I_d and c for the fastest response.

However, even if this process will highlight the fastest response, it won't tell anything about the robustness of the system. For this reason we've also analyzed the time and frequency response of the linearized system.

Linearized system

Before linearizing we make another observation. As we have noticed before, the system is only locally stable, spinning around the *positive* or *negative* direction of the major principal axis of inertia, regardless of the sign but depending only on initial conditions. In fact, if we consider the separatrices in Figure 5.2, for initial conditions in the lateral quadrants, due to energy dissipation the angular momentum vector may follow a path leading to e_3 or $-e_3$.

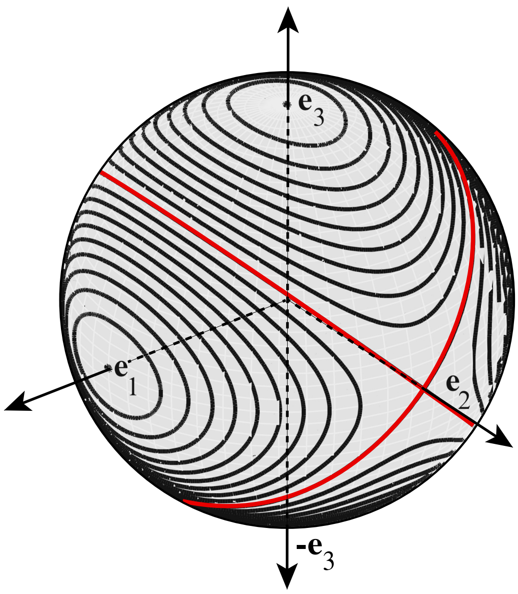

Figure 5.2: Constant energy paths on the angular momentum sphere for a triaxial inertia ratios $J_1 < J_2 < J_3$.

If we want to achieve a global asymptotic stability and increase the probability to spin around the positive major principal axes, we can add another fictional disc spinning in the body z-axis direction using the superspin principle. The disc spin rate will be such that:

$$\sigma = \frac{I_s}{I_t} > 1.2 \tag{5.21}$$

where I_s is the inertia of the spin axis and I_t is the inertia of the transverse axis (considering, at this stage, an axialsymmetric distribution of mass). With the addition of the spinning disc, the effective spin axis inertia and the inertia rate respectively become:

$$I_{s_{eff}} = I_s + \frac{|h_s|}{\Omega} \tag{5.22}$$

$$\sigma_{eff} = \frac{I_s + \frac{|h_s|}{\Omega}}{I_t} \tag{5.23}$$

where Ω is the spin rate and h_s is the projection of h along the major principal axis. From (5.23) we get h_s:

$$h_s > (1.2 I_t - I_s)\Omega = h_0 \tag{5.24}$$

With the addition of the spinning disc (4.9) becomes:

$$\mathbf{I}_b \dot{\boldsymbol{\omega}}_n^b + \boldsymbol{\omega}_n^b \times \mathbf{I}_b \boldsymbol{\omega}_n^b + \dot{\mathbf{h}} + \boldsymbol{\omega}_n^b \times \mathbf{h} = -\boldsymbol{\tau}_d \tag{5.25}$$

where $\mathbf{h} = h_0$ as defined in (5.24). Now, we can also evaluate the stability of the corresponding linear system by linearizing the equations (4.8), (4.9), along with (4.7), around the equilibrium point where:

$$\begin{array}{rcl} \boldsymbol{\omega}_n^b &=& \boldsymbol{\omega}_0 + \delta\boldsymbol{\omega}_n^b \\ \boldsymbol{\omega}_n^d &=& \boldsymbol{\omega}_0 + \delta\boldsymbol{\omega}_n^d \\ \mathbf{h} &=& \mathbf{h_0} + \delta\mathbf{h}_0 \end{array} \tag{5.26}$$

where:

$$\boldsymbol{\omega}_0 = \boldsymbol{\omega}_{n_{eq}}^b = \boldsymbol{\omega}_{n_{eq}}^d = \Omega \mathbf{e}_z \tag{5.27}$$

with $\mathbf{e}_z$ corresponds to the principal axis of inertia, as previously defined.
Using the Taylor expansion series for the nonlinear terms in both the equations:

$$f(\boldsymbol{\omega}_n^b, \boldsymbol{\omega}_n^d) \simeq f(\boldsymbol{\omega}_0) + \frac{\partial}{\partial \boldsymbol{\omega}_n^b} f \cdot \delta\boldsymbol{\omega}_n^b + \frac{\partial}{\partial \boldsymbol{\omega}_n^d} f \cdot \delta\boldsymbol{\omega}_n^d \tag{5.28}$$

or basically applying the Jacobian linearization:

$$\mathbf{J} = \begin{bmatrix} \left.\frac{\partial f}{\partial \omega_n^b}\right|_{\omega_0} & \left.\frac{\partial f}{\partial \omega_n^d}\right|_{\omega_0} \\ \left.\frac{\partial g}{\partial \omega_n^b}\right|_{\omega_0} & \left.\frac{\partial g}{\partial \omega_n^d}\right|_{\omega_0} \end{bmatrix} \tag{5.29}$$

we can get the system of equation into the closed loop state space form:

$$\dot{\mathbf{x}} = A\mathbf{x} \tag{5.30}$$

where A is:

$$A = \begin{bmatrix} -\mathbf{I}_b^{-1}\left[\boldsymbol{\omega}_0^{\times}\mathbf{I}_b - (\mathbf{I}_b\boldsymbol{\omega}_0 + \mathbf{h}_0)^{\times} + c\right] & \mathbf{I}_b^{-1}c \\ -\mathbf{I}_d^{-1}\left[-(\mathbf{I}_d\boldsymbol{\omega}_0)^{\times} - c\right] & -\mathbf{I}_d^{-1}\left(\boldsymbol{\omega}_0^{\times}\mathbf{I}_\mathbf{d} + c\right) \end{bmatrix} \tag{5.31}$$

is a 6×6 matrix and $\dot{\mathbf{x}}$ and $\mathbf{x}$ are:

$$\dot{\mathbf{x}} = \begin{bmatrix} \delta\dot{\boldsymbol{\omega}}_n^b \\ \delta\dot{\boldsymbol{\omega}}_n^d \end{bmatrix} \qquad \mathbf{x} = \begin{bmatrix} \delta\boldsymbol{\omega}_n^b \\ \delta\boldsymbol{\omega}_n^d \end{bmatrix}$$

or in the open loop form:

$$\begin{aligned} \dot{\mathbf{x}} &= A\,\mathbf{x} + B\,\mathbf{u} \\ \mathbf{u} &= -K\mathbf{x} \\ \mathbf{y} &= C\,\mathbf{x} + D\,\mathbf{u} \end{aligned} \tag{5.32}$$

where A and B respectively are:

$$A = \begin{bmatrix} -\mathbf{I}_b^{-1}\left[\boldsymbol{\omega}_0^{\times}\mathbf{I}_b - (\mathbf{I}_b\boldsymbol{\omega}_0 + \mathbf{h}_0)^{\times}\right] & \mathbf{0} \\ \mathbf{I}_d^{-1}(\mathbf{I}_d\boldsymbol{\omega}_0)^{\times} & -\mathbf{I}_d^{-1}\left(\boldsymbol{\omega}_0^{\times}\mathbf{Id}\right) \end{bmatrix} \tag{5.33}$$

$$B(-K) = \begin{bmatrix} -\mathbf{I}_b^{-1}c & \mathbf{I}_b^{-1}c \\ \mathbf{I}_d^{-1}c & -\mathbf{I}_d^{-1}c \end{bmatrix} \tag{5.34}$$

and, since we are only interested in the spacecraft angular velocity, the matrices C and D are:

$$C = \begin{bmatrix} 1 & 0 & 0 & 0 & 0 & 0 \\ 0 & 1 & 0 & 0 & 0 & 0 \\ 0 & 0 & 1 & 0 & 0 & 0 \\ 0 & 0 & 0 & 0 & 0 & 0 \\ 0 & 0 & 0 & 0 & 0 & 0 \\ 0 & 0 & 0 & 0 & 0 & 0 \end{bmatrix}; \quad D = [\mathbf{0}] \tag{5.35}$$

In order to study the behavior of the feedback controller, we may identify the matrices B and K as:

$$B = \begin{bmatrix} \mathbf{I}_b^{-1} & \mathbf{0} \\ \mathbf{0} & \mathbf{I}_d^{-1} \end{bmatrix}; \quad K = \begin{bmatrix} \mathbf{c} & -\mathbf{c} \\ -\mathbf{c} & \mathbf{c} \end{bmatrix} \tag{5.36}$$

From this point, for simplicity, we can consider:

$$\mathbf{I}_b = \begin{bmatrix} I_t & 0 & 0 \\ 0 & I_t & 0 \\ 0 & 0 & I_s \end{bmatrix} \tag{5.37}$$

with I_t the greater transverse inertia moment and h_0 is defined as (5.24). We can now find the closed loop A matrix by substituting the following terms in (5.33):

$$\begin{aligned} \boldsymbol{\omega}_0^{\times} &= \begin{bmatrix} 0 & -\Omega & 0 \\ \Omega & 0 & 0 \\ 0 & 0 & 0 \end{bmatrix} \quad \longrightarrow \quad \boldsymbol{\omega}_0^{\times}\mathbf{I}_b = \begin{bmatrix} 0 & -\Omega I_t & 0 \\ \Omega I_t & 0 & 0 \\ 0 & 0 & 0 \end{bmatrix} \\ \mathbf{I}_b\boldsymbol{\omega}_0 &= \begin{bmatrix} 0 \\ 0 \\ \Omega I_s \end{bmatrix} \quad \longrightarrow \quad (\mathbf{I}_b\boldsymbol{\omega}_0)^{\times} = \begin{bmatrix} 0 & -\Omega I_s & 0 \\ \Omega I_s & 0 & 0 \\ 0 & 0 & 0 \end{bmatrix} \end{aligned} \tag{5.38}$$

$$A = \begin{bmatrix} 0 & -\Gamma & 0 & 0 & 0 & 0 \\ \Gamma & 0 & 0 & 0 & 0 & 0 \\ 0 & 0 & 0 & 0 & 0 & 0 \\ 0 & -\Omega & 0 & 0 & \Omega & 0 \\ \Omega & 0 & 0 & -\Omega & 0 & 0 \\ 0 & 0 & 0 & 0 & 0 & 0 \end{bmatrix} \tag{5.39}$$

where Γ is defined as:

$$\Gamma = -\Omega + \frac{(\Omega I_s + h_0)}{I_t} \tag{5.40}$$

and B becomes:

$$B = \begin{bmatrix} 1/I_t & 0 & 0 & 0 & 0 & 0 \\ 0 & 1/I_t & 0 & 0 & 0 & 0 \\ 0 & 0 & 1/I_s & 0 & 0 & 0 \\ 0 & 0 & 0 & 1/I_d & 0 & 0 \\ 0 & 0 & 0 & 0 & 1/I_d & 0 \\ 0 & 0 & 0 & 0 & 0 & 1/I_d \end{bmatrix} \tag{5.41}$$

The transfer function for the autonomous linear systems can be found by taking the Laplace transform [15] of both sides of the first and third equations in (5.32) with zero initial conditions:

$$s\mathbf{x}(s) = A\mathbf{x}(s) + B\mathbf{u}(s) \tag{5.42}$$

$$\mathbf{y}(s) = C\mathbf{x}(s) + D\mathbf{u}(s) \tag{5.43}$$

where s is the Laplace variable. Solving for $\mathbf{x}(s)$ yields to:

$$\mathbf{y}(s) = \left[C\,(s\mathbf{I} - A)^{-1}\,B + D\right]\mathbf{u}(s) \tag{5.44}$$

Thus, the plant transfer function becomes:

$$\frac{\mathbf{y}(s)}{\mathbf{u}(s)} = \left[C\,(s\mathbf{I} - A)^{-1}\,B + D\right] \tag{5.45}$$

The gain c has been selected by evaluating the time performance of the isolated SISO system for the first variable of $\mathbf{y}$ and then system performances have been evaluated for the complete MIMO system. From (5.45), isolating only the first SISO we evaluate the *plant* transfer function:

$$y_{1,1}(s) = \frac{s}{I_t(\Gamma^2 + s^2)}u_{1,1}(s) \tag{5.46}$$

where

$$G_{p_{1,1}}(s) = \frac{s}{I_t(\Gamma^2 + s^2)} \tag{5.47}$$

Considering the input as a state error feedback as said in Section 4.1.3:

$$\mathbf{u}(t) = -c\left(\boldsymbol{\omega}_n^b - \boldsymbol{\omega}_n^d\right) = c\,(r(t) - y(t)) = ce(t) \tag{5.48}$$

$$\mathbf{u}(s) = c\mathbf{e}(s) = c\,(r(s) - y(s)) \tag{5.49}$$

where $e(t)$ is the error signal and

$$G_c(s) = c \tag{5.50}$$

is the *controller* transfer function. Rearranging (5.46) and (5.49) we have:

$$y(s) = \frac{G_c(s)G_p(s)}{1 + G_c(s)G_p(s)}r(s) \tag{5.51}$$

where the closed-loop transfer function is:

$$T(s) = \frac{G_c(s)G_p(s)}{1 + G_c(s)G_p(s)} = \frac{c/I_t \cdot s}{s^2 + (c/I_t)s + \Gamma^2} \tag{5.52}$$

We can now select a value for the gain by studying the step response of the system. Also, we notice that the value of c from the numerical optimization are not the optimum in the linearized system. In fact, for the SISO system we have:

c	I_d	Settling time (t_s) [s]	poles	zero
0.41837	0.0082551	~ 600	-219.9458 -0.0065	0

Table 5.2: Settling time, poles and zero of the SISO System with the c gain from the numerical optimization.

As we can see from Table 5.2 one of the system poles is too close to the zero of the transfer function and the other is too far from the origin. By analizing the root locus of the system as a function of c, we find that the optimum for the SISO system is achieved with two orders of magnitude less than the previous. Also, as we can see from Table 5.3 and Figure 5.3, both poles are complex and far enough from the zero.

c	I_d	Settling time (t_s) [s]	poles	zero
0.0041776	0.0021388	4.91	$-1.0982 \pm 0.4838i$	0

Table 5.3: Settling time, poles and zero of the SISO System with optimized c gain.

It's interesting to note that the nonlinear controller is optimal at a very different value of "c" from the linear controller. This difference is due to the fact that, in the linear controller the nonlinear optimum value is still stable but the poles of the linearized system become all real and one moves to zero, when the other moves further away on the left hand plane, as we see in Table 5.2, making the system "faster" but less robust. The chosen values in Table 5.3 are close to the limit when the two poles become aperiodic (both real with zero imaginary part), but still are two complex conjugates as we can see from the root locus in Figure 5.3. Now we can evaluate the MIMO performance in terms of transient time specification (in particular settling time) as well as frequency response in Figures 5.4 and 5.5.
From Figure 5.4 we notice that all of the multi-input/multi-output system settles in $t_s < 2s$ and, from Figure 5.5 we see that for all of them the magnitude never crosses the zero because always negative. Such systems are always stable. Moreover, the phase never touches -180 deg, another indication that the system is stable. Even though the linearized answer may be helpful for control design, we should keep in mind that the nonlinear system guarantees stability for a larger nonlinear basin of attraction (very different initial conditions), regardless of the design.

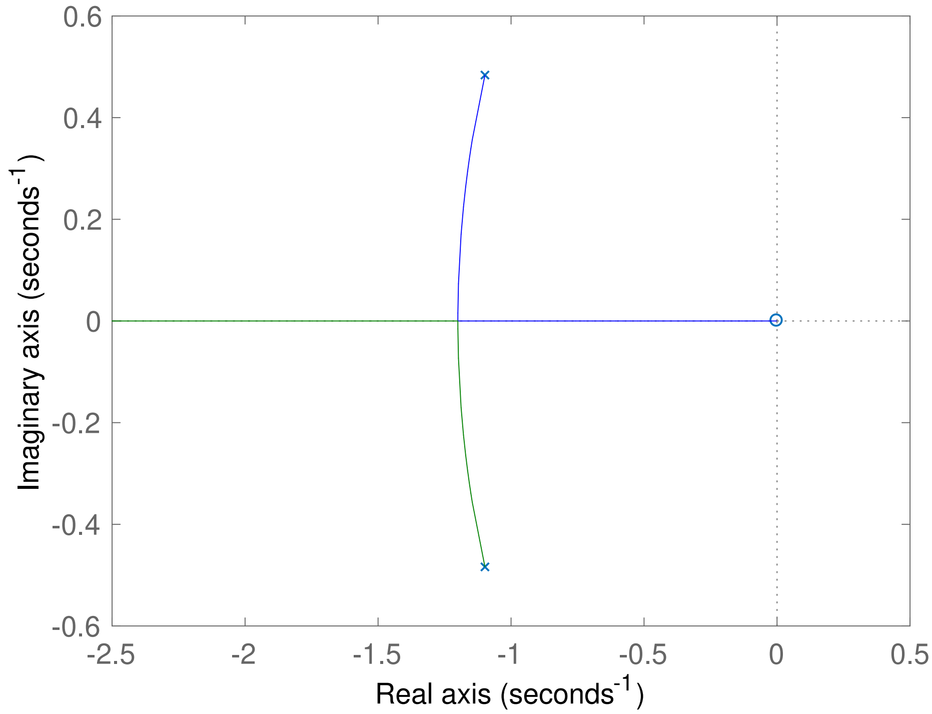

Figure 5.3: Root locus for SISO system.

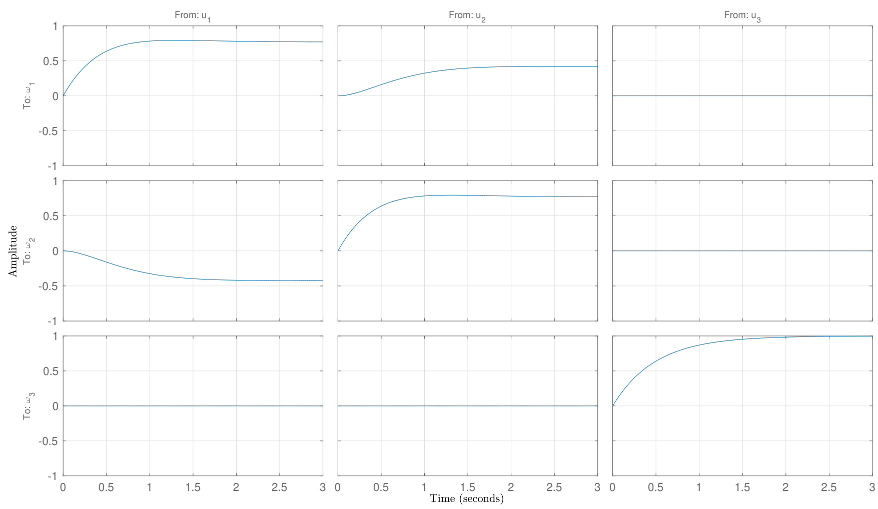

Figure 5.4: Step plot for the MIMO system.

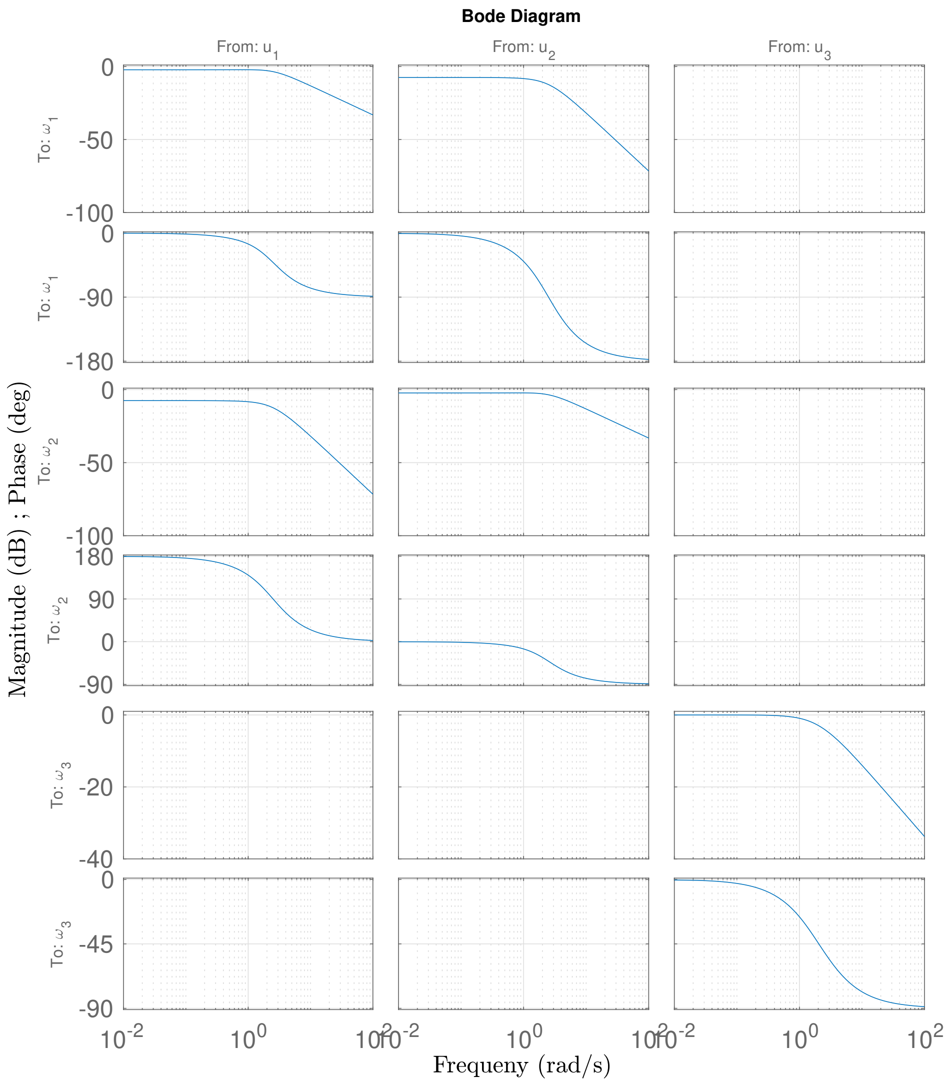

Figure 5.5: Bode Magnitude and Phase plot for the MIMO system.

5.2.3 Pointing controller

Now we can analyze the stability of the pointing controller. As said before, this controller is based on the assumption that spinning stability is already achieved and this was the starting point in the design of the slew controller. Another assumption we make for this controller is for small angles and rates.

Because of this we may write:

$$\begin{bmatrix} \omega_x \\ \omega_y \\ \omega_z \end{bmatrix} = \begin{bmatrix} \dot{\psi} \\ \dot{\theta} \\ \dot{\varphi} \end{bmatrix} \tag{5.53}$$

which substituted in (4.27) yields to:

$$\begin{aligned} I_x\ddot{\psi} &= T_{cx} + T_{dx}, \\ I_y\ddot{\theta} &= T_{cy} + T_{dy}, \\ I_z\ddot{\varphi} &= T_{cz} + T_{dz}. \end{aligned} \tag{5.54}$$

We can write (5.54) in compact form as:

$$I\ddot{\theta} = T_c + T_d \tag{5.55}$$

In this case, as done for the Kane Damper linear model, we identify the plant and controller transfer functions. For the plant, applying the Laplace transform to (5.55), we have:

$$G_p(s) = \frac{1}{Is^2} \tag{5.56}$$

and for the controller, applying the Laplace transform to (4.32):

$$G_c(s) = K_p + sK_d \tag{5.57}$$

Where in this case the error is the angle θ_e between the spin axis and the local magnetic field. As before, the poles of the closed-loop transfer function:

$$T(s) = \frac{G_c(s)G_p(s)}{1 + G_c(s)G_p(s)} \tag{5.58}$$

must have at least negative real parts. Substituting (5.56) and (5.57) into (5.58) we have:

$$T(s) = \frac{G_c(s)G_p(s)}{1 + G_c(s)G_p(s)} = \frac{(K_p + sK_d)/(Is^2)}{1 + (K_p + sK_d)/(Is^2)} = \frac{s(K_d/I) + (K_p/I)}{s^2 + s(K_d/I) + (K_p/I)} \tag{5.59}$$

we define

$$\omega_n^2 = \frac{K_p}{I}, \qquad 2\zeta\omega_n = \frac{K_d}{I}$$

where ω_n is the undamped natural frequency and ζ is the damping ratio. The (5.59) becomes:

$$T(s) = \frac{2\zeta\omega_n s + \omega_n^2}{s^2 + 2\zeta\omega_n s + \omega_n^2} \tag{5.60}$$

as we can see, the PD is a second order system. The closed-loop poles are:

$$s_{1,2} = -\zeta\omega_n \pm \omega_n\sqrt{\zeta^2 - 1}$$

Among the three possible solution ($0 < \zeta < 1, \quad \zeta = 1, \quad \zeta > 1$) we are interested in the first one, for which the system is called underdamped. In this case we allow the system to have an overshoot and an oscillatory behavior although it provides a faster response. In this case the poles are two complex conjugate:

$$s_{1,2} = -\zeta\omega_n \pm j\omega_d \tag{5.61}$$

where $\omega_d = \omega_n\sqrt{1-\zeta^2}$ is the damped natural frequency. These poles lead to decaying oscillatory behavior at frequency ω_d.
We are studying the step response, to a reference command

$$R(s) = \frac{1}{s}$$

that yields to:

$$Y(s) = \frac{2\zeta\omega_n s + \omega_n^2}{s^2 + 2\zeta\omega_n s + \omega_n^2}\frac{1}{s} \tag{5.62}$$

Taking the inverse Laplace transform of (5.62) we obtain the step response in the time-domain:

$$y(t) = 1 - e^{-\zeta\omega_n t}\left[\cos\omega_d t - \frac{\zeta\omega_n}{\omega_d}\sin\omega_d t\right] \tag{5.63}$$

With this equation we can now define ω_n and ζ by selecting a proper behavior using a number of time-domain specification among the following:

- **Rise time** t_r - Time to first reach the final value;
- **Peak time** t_p - Time to reach the first peak;
- **Maximum overshoot** M_p - Maximum overshoot from the final value (percentage);
- **Settling time** t_s - Time to get to 2% of the final value and stay.

We report the expression related to these specifications for a standard second order system:

$$
\begin{aligned}
t_r &= t\,\big|_{y(t)=1} = \frac{\pi - \beta}{\omega_d} \qquad \text{where} \qquad \beta = \tan^{-1}\left(\frac{\sqrt{1-\zeta^2}}{\zeta}\right) \\
t_p &= t\,\big|_{\frac{dy(t)}{dt}=0} = \frac{\pi}{\omega_d} \\
M_p &= y_p\big|_{t=t_p} = e^{-\pi\zeta/\sqrt{1-\zeta^2}} \times 100\% \\
t_s &= \frac{\ln\left(0.02\sqrt{1-\zeta^2}\right)}{-\zeta\omega_n} \approx \frac{4.4}{\zeta\omega_n}
\end{aligned}
$$

However (5.63) is not a standard second order system due to the presence of a closed loop zero but, as the zero location moves to infinity, its influence on the system transient behaviour decreases. Moreover, since we want closed loop poles to have negative real part (for asymptotic stability) $\zeta\omega_n > 0$ and also $a = \omega_n/2\zeta > 0$ so the system will have a closed loop zero in the left half plane. The effect of a LHP zero is to increase the overshoot, decrease the peak time, and decrease the rise time; the settling time is not affected too much. In other words, a LHP zero makes the step response faster. In general we prefer to have the closed loop zero far away from the poles in order to have no significant effect on the transient behavior. With the previous, given some specification, we are able to find the allowable region for the closed-loop poles by selecting their maximum value or the exact value of two of them. In particular, by choosing a peak time and a settling time we lock the values of ζ and ω_n of the standard second order system.
The steps to be followed are:

- Select a desired transient response behavior and localize the dominant closed-loop poles;
- Analyze the Characteristic equation ($1 + G_0(s) = 0$) for the desired control law;
- Design the proper gains via the root locus method to ensure the desired dominant poles lie on the root locus.

For the design of the K_d and K_p gains, we'll use peak time and settling time specifications. In particular, we'll get them as a multiple of the orbital period. Since the the controller works best in LEO orbits, we decided to use in the simulation the following orbital parameters as in Table: where T in Table 5.4

altitude (a) [km]	200
inclination i [deg]	10
Earth's radius [km] Re	6371
Gravitational parameter μ [kg^3s^{-1}]	398600
Orbital period T [s]	5301

Table 5.4: Orbital parameters and constants for the simulation.

is calculated as:

$$T = 2 \cdot \pi \sqrt{\frac{(Re + a)^3}{\mu}} \tag{5.64}$$

We now get t_p and t_s as:

$$t_p = 1.8 \cdot T = \frac{\pi}{\omega_d} \longrightarrow \omega_d = \frac{pi}{t_p}$$

$$t_s = 2 \cdot T = \frac{4.4}{\zeta\omega_n} \longrightarrow \zeta\omega_n = \frac{4.4}{t_s}$$

where ω_d and $\zeta\omega_n$ are respectively the imaginary and real part of the closed loop poles:

$$s_{1,2} = -\zeta\omega_n \pm j\omega_d = (-0.4150 \pm 0.3292i) \cdot e^{-3}$$

Lets recall the controller and plant transfer function:

$$G_c(s) = K_p + sK_d = K_{pd}\left(s + \frac{1}{T}\right) \qquad G_p(s) = \frac{1}{Is^2}; \tag{5.65}$$

and the closed-loop transfer function is:

$$T(s) = \frac{G_c(s)G_p(s)}{1 + G_c(s)G_p(s)}$$

The closed loop poles satisfy the characteristic equation:

$$1 + G_c(s)G_p(s) = 0 \quad \longrightarrow \quad G_c(s)G_p(s) = -1$$

The above equation must satisfy the angle condition:

$$\sphericalangle G_c(s_{1,2}) + \sphericalangle G_p(s_{1,2}) = \sphericalangle -1 = (2n+1)\pi \tag{5.66}$$

where:

$$\phi_p = 180^\circ - \tan^{-1}(\Im(s)/\Re(s)) = 180 - 218.4261 = -38.4261^\circ$$

$$\sphericalangle G_p(s_1) = \sphericalangle\left(\frac{1}{s^2}\right) = -2\phi_p = 76.8521^\circ$$

$$\sphericalangle G_c(s_1) = -180^\circ - \sphericalangle G_p(s_1) = -180^\circ - 76.8521^\circ = 103.1479^\circ$$

We have

$$\tan \psi_{pd} = \frac{\Im(s_1)}{1/T - \Re(s_1)}$$

which rearranges to give:

$$\frac{1}{T} = \frac{\Im(s_1)}{\tan(103.1479°)} - \Re(s_1) = 3.38 \cdot e^{-4}; \quad \rightarrow T = 2.96 \cdot e^{3};$$

Now we can evaluate the characteristic equation:

$$1 + G_c(s)G_p(s) = 1 + K_{pd}\left(s + \frac{1}{T}\right)\left(\frac{1}{Is^2}\right) = 0$$

That means:

$$K_{pd} = \left|\frac{Is^2}{s + 1/T}\right| \tag{5.67}$$

that, evaluated at $s_1 = (-0.4150 + 0.3292i) \cdot e^{-3}$, with $I = 1kg \cdot m^2$ gives:

$$K_{pd} = 8.303 \cdot e^{-4}$$

The corresponding PD gains are:

$$K_d = K_{pd} = 8.303 \cdot e^{-4}, \qquad K_p = K_{pd}/T = 2.806 \cdot e^{-7}. \tag{5.68}$$

Lets recall the transfer function:

$$T(s) = \frac{G_c(s)G_p(s)}{1 + G_c(s)G_p(s)} = \frac{(K_p + sK_d)/Is^2}{1 + K_p + sK_d)/Is^2} = \frac{s(K_d/I) + (K_p/I)}{s^2 + s(K_d/I) + (K_p/I)}$$

Which will be multiplied by I_b in the controller. As we can see in Figure 5.6 the presence of a zero affects the peak response, resulting in an overshoot and in a faster response, but not the settling time. A frequency response analysis has been operated on the PD control law to ensure stability margins. It turns out that the system is stable, with infinite gain margin, since the phase never crosses $-180°$, as we can see in Figure 5.7.

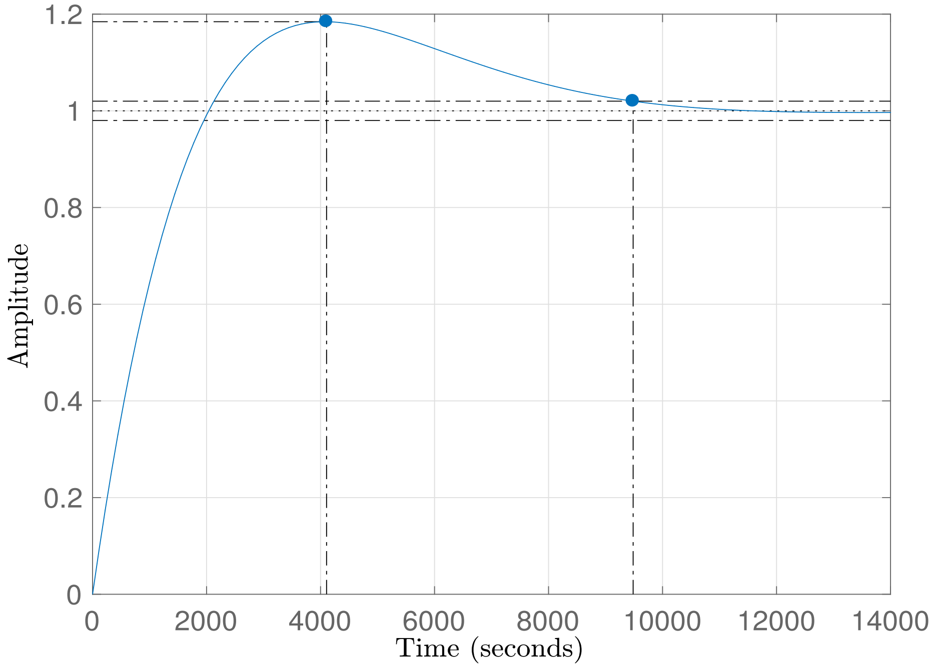

Figure 5.6: Step response for PD pointing controller.

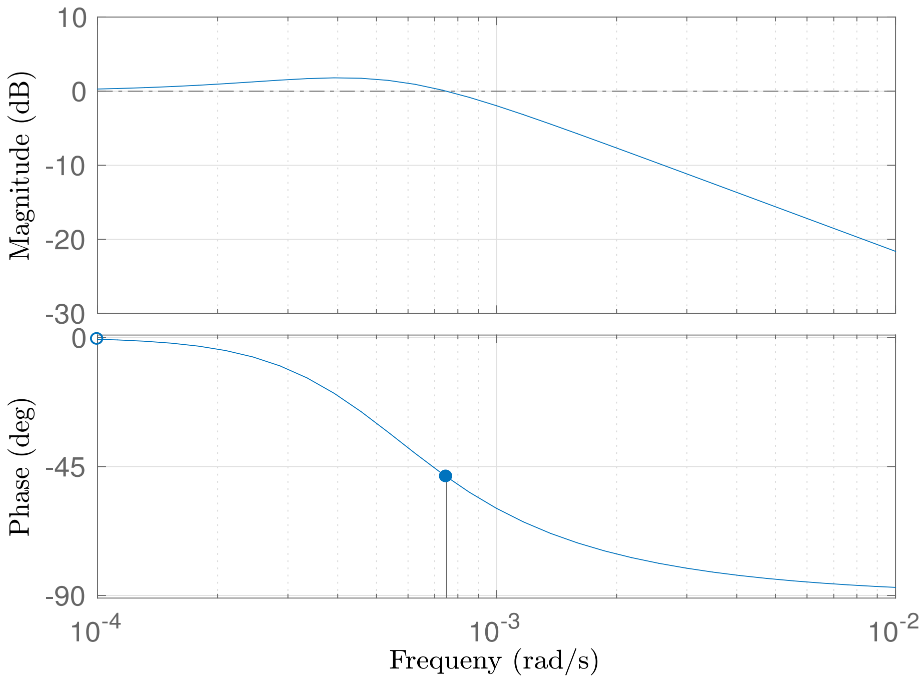

Figure 5.7: Bode plot for PD pointing controller.

Chapter 6

Simulation and results

In this section will be presented the steps followed to simulate the control system. This was achieved by the use of MATLAB SIMULINK to simulate all the external variables, such as the spacecraft dynamics and kinematics, the disturbance torques, the orbital dynamics and the Earth's magnetic dipole model, as well as the control torques, giving as an output the actual torque and the required current to be sent to the magnetorquers. The initial conditions are given via a MATLAB script, that was also used in the post processing phase to analyze the results. After assessing the SIMULINK model, the code was translated in C++ via the autocode feature of SIMULINK and simulated on two Arduino based boards (namely, two Adafruit Feather M0 Adalogger), one of them (the *Universe* board) simulating all the external variables, and one (the actual ACS flight computer) addressed to the control torques (and current) simulation only. For the sampling time in the fixed step integration, it was chosen not to have a time step lower than 0.01 (100Hz) that will represent the time step in the discrete time integration.

6.1 Simulation

First were simulated the spacecraft dynamics and kinematics as in sections 2.2.1 and 2.2.2. Even though the controller doesn't uses the kinematics the attitude is required in the simulation to simulate the actual magnetic field in the body coordinate frame. The dynamic model in Figure 6.1 simply integrates the (2.19) while considering the inertia matrix in the body frame. The SIMULINK model for the kinematics in Figure 6.2 uses the formulation in [27] and [3] for the quaternion integration from angular velocity:

$$\dot{q} = \frac{1}{2}\Omega q \tag{6.1}$$

where:

$$\Omega = \begin{bmatrix} 0 & -\omega_x & -\omega_y & -\omega_z \\ \omega_x & 0 & \omega_z & -\omega_y \\ \omega_y & -\omega_z & 0 & \omega_x \\ \omega_z & \omega_y & -\omega_x & 0 \end{bmatrix} \tag{6.2}$$

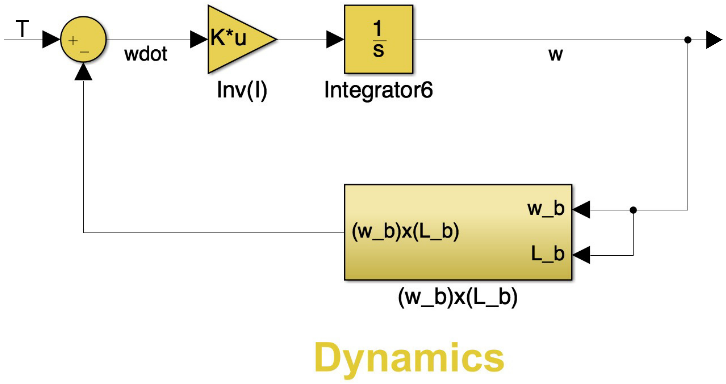

Figure 6.1: Dynamics model in Simulink.

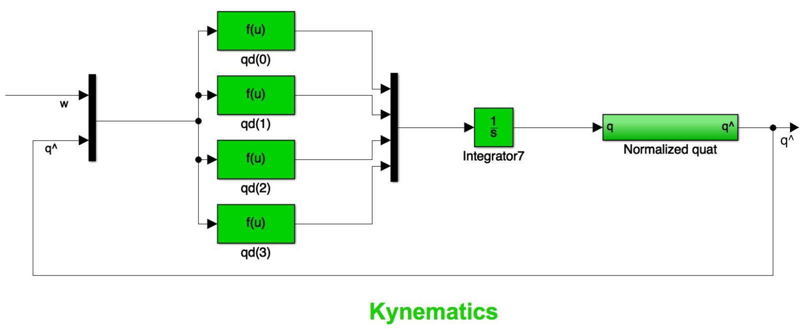

Figure 6.2: Kinematics model in Simulink.

On the other hand, the magnetic field has been evaluated in ECI coordinate frame by using the spacecraft orbital dynamics as in Figures 6.3 and 6.4 Then, the attitude has been used to evaluate the external magnetic field in the body coordinate system, as the magnetometer would do. Finally the two control laws have been introduced, which use both the spacecraft angular velocity and the magnetic field in the body frame as input.

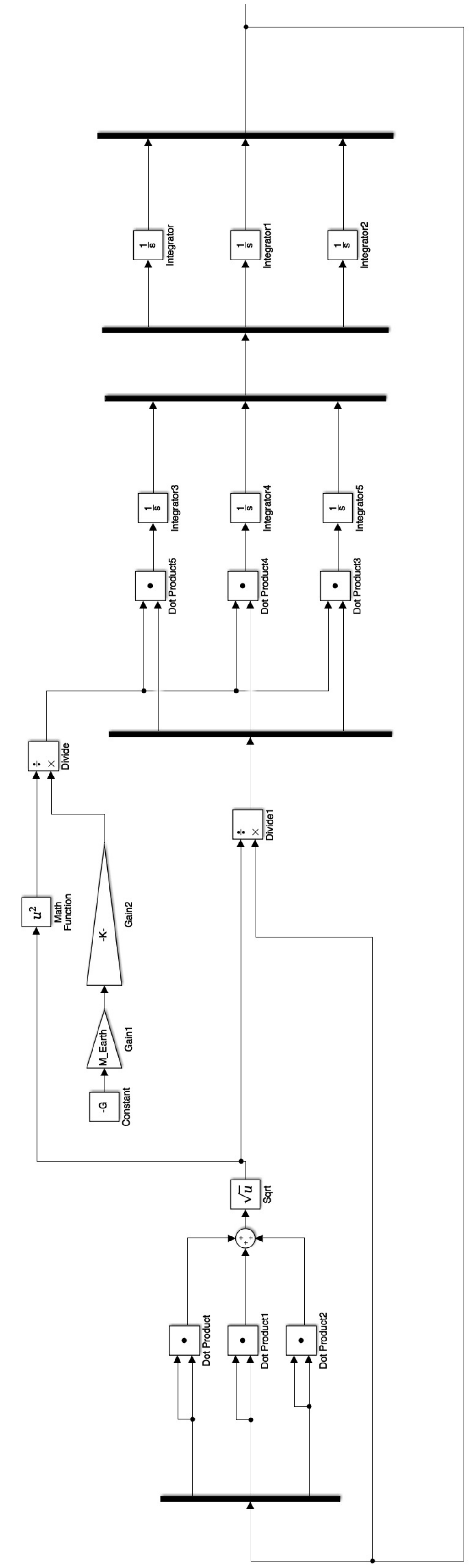

Figure 6.3: Orbital dynamic model in Simulink.

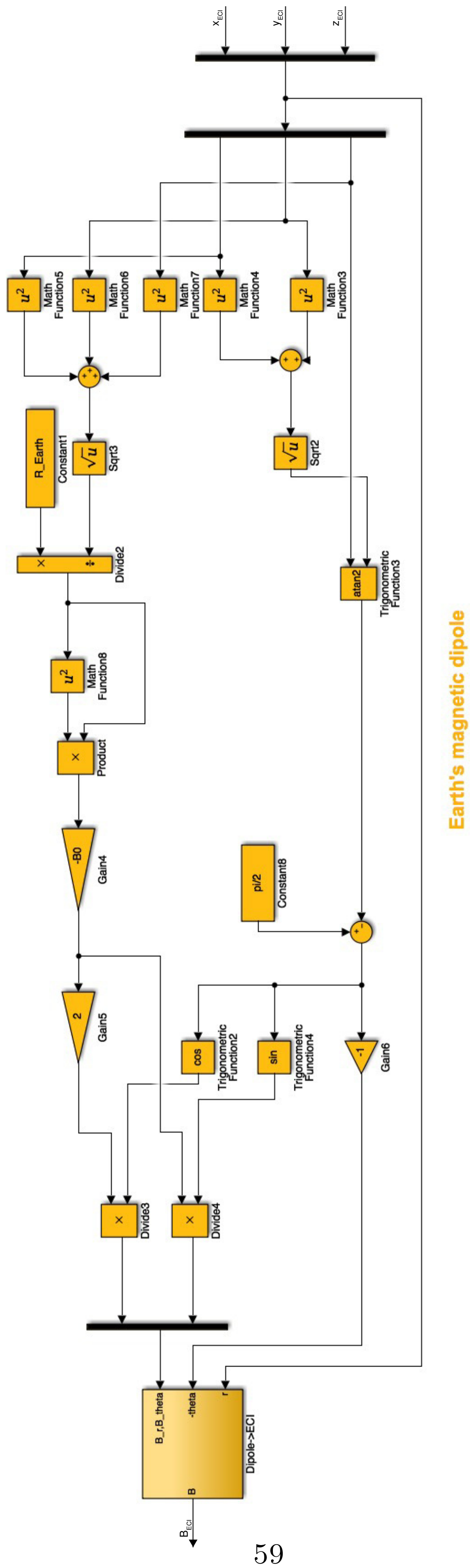

Figure 6.4: Earth's magnetic field dipole model in ECI frame.

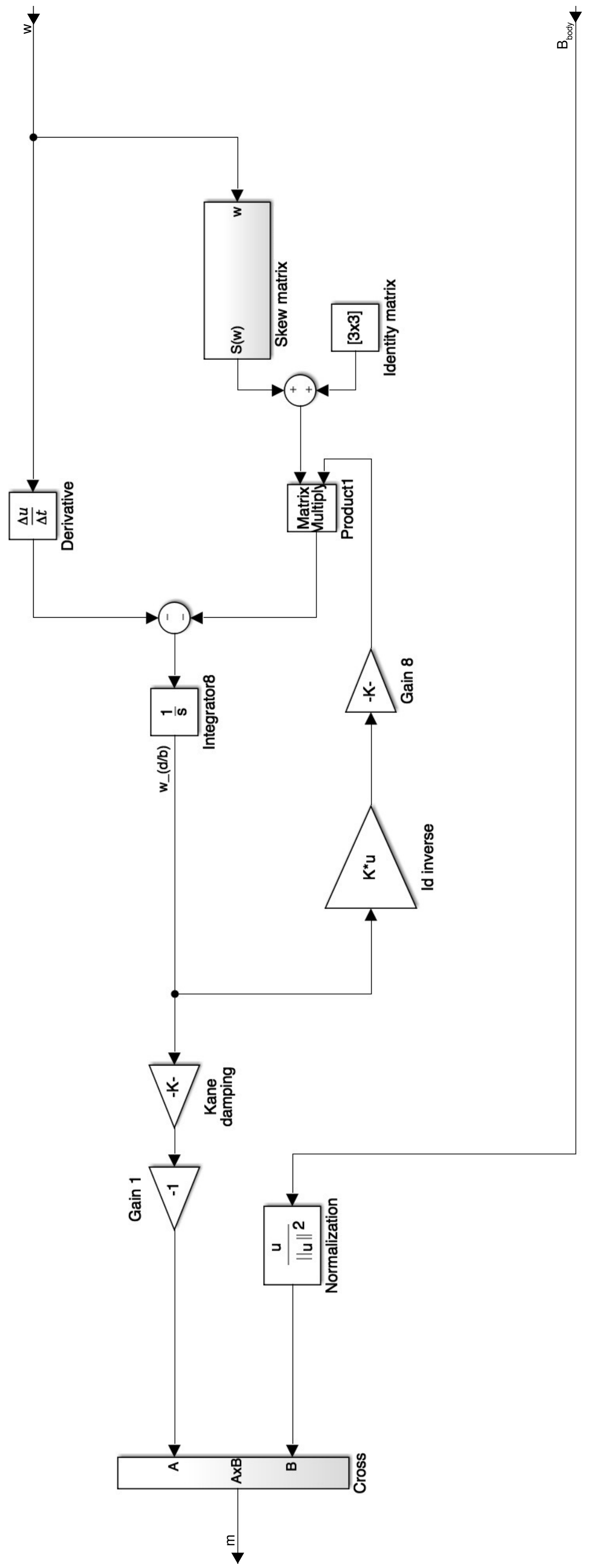

Figure 6.5: Kane damper non-linear controller model.

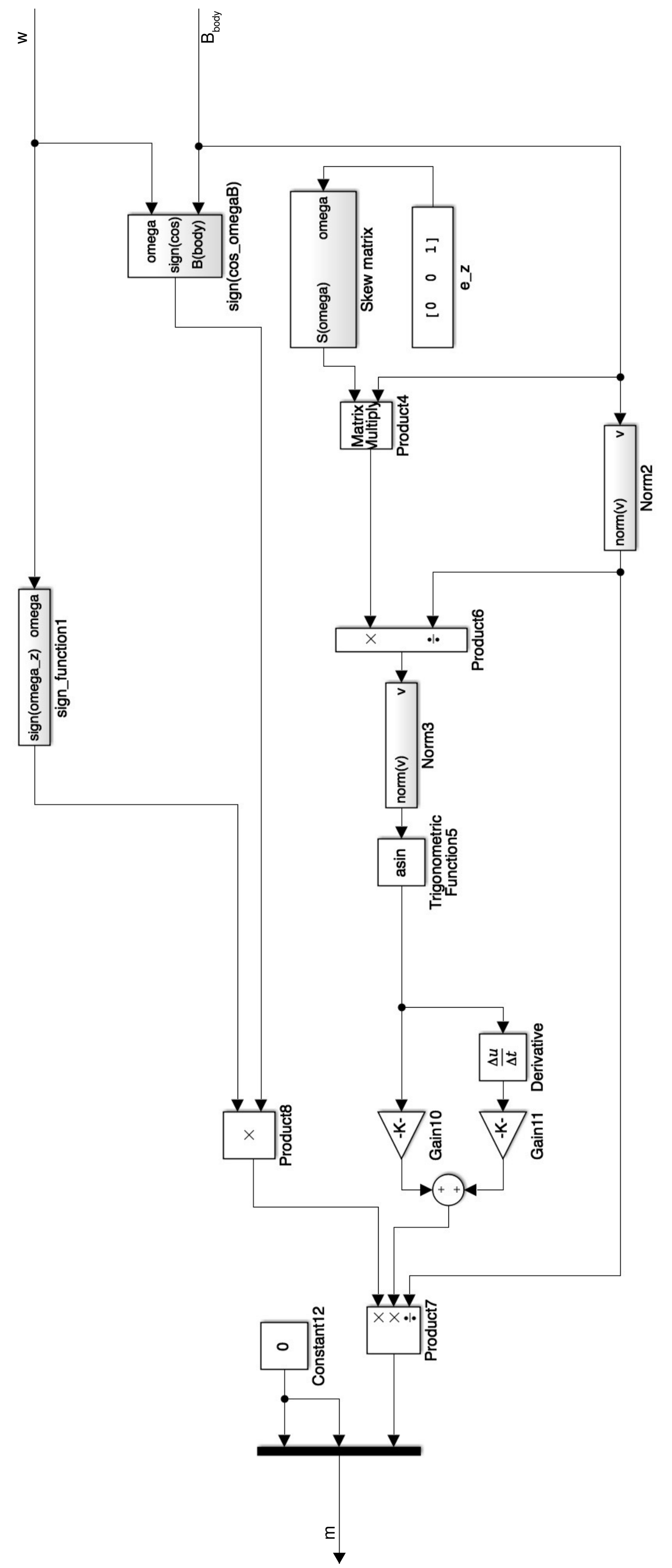

Figure 6.6: Pointing controller model.

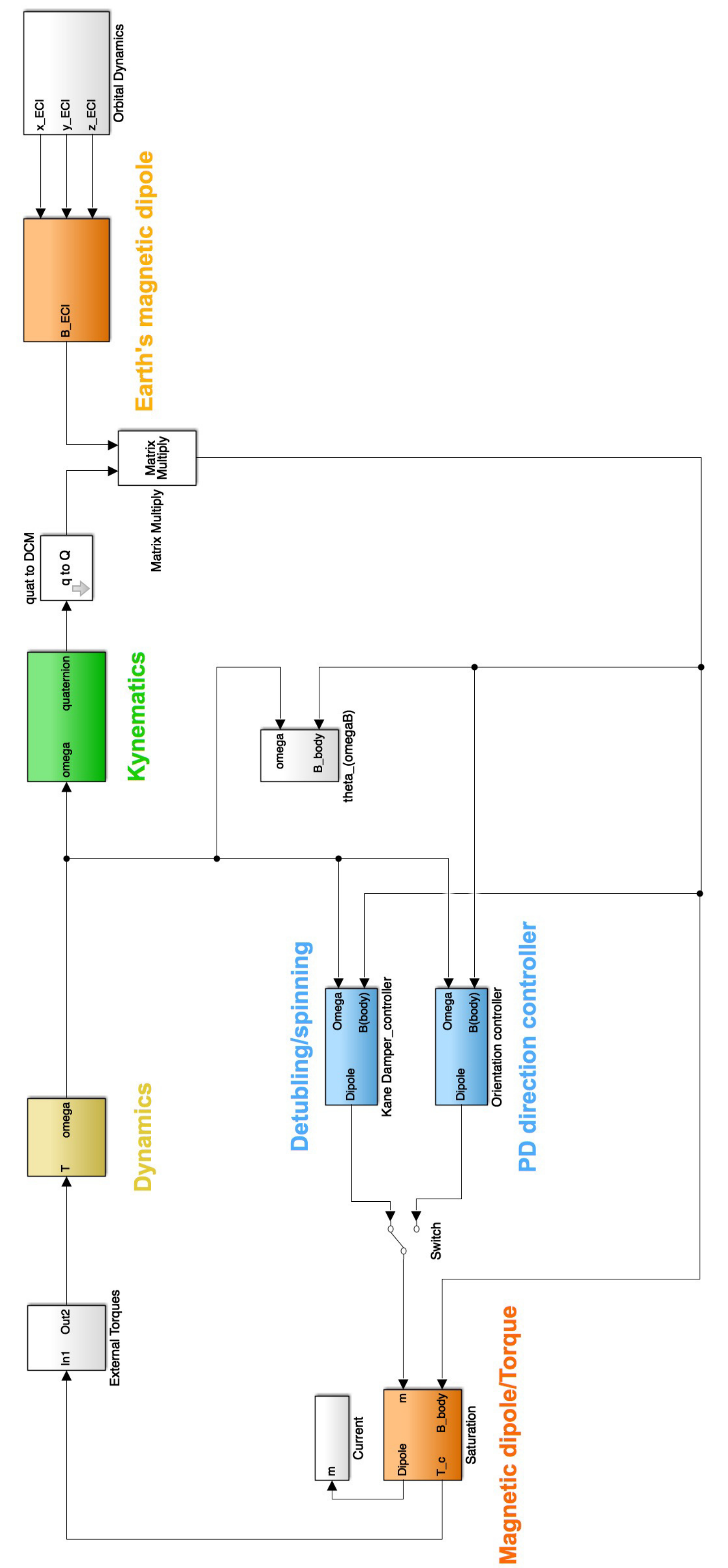

Figure 6.7: Complete simulation model.

The dipole moment produced is then processed through a saturation cap, which limits the produced torque with the actuators capability, as we can see in the compact complete model in Figure 6.7. Also, as we notice, the model outputs the current that will be needed by the magnetorquers. Furthermore, both the control laws will be run at the same time and, based on the dynamics, one will be used rather than the other. In particular, the first controller will be on until the angular velocity aligns with the major principal axis of inertia. Then the controller will be switched to the pointing/direction controller. In the SIMULINK model this is done manually but while coding it in the flight computer it has been implemented a switching condition.

6.2 Results

In this section are presented the results, time performance and accuracy for both nutation damper and pointing controller. In particular, for the nutation damper controller, only the results relative to the kane damper are presented. Also, since at the time this work is done the real magnetorquers are not available, the data for the maximum magnetic dipole generated by the magnetorquers (assumed to be the same for all three magnetorquers), comes from external measurements of the generated magnetic dipole of some magnetorquers similar to those that are going to be used for this project. Rather than relying on the (3.5), the actual maximum magnetic dipole that can be generated has been evaluated experimentally giving:

$$m = 0.02 \quad [A \cdot m^2] \tag{6.3}$$

that is way lower than expected in the first time. For this reason, for the pointing controller, are presented the results with and without that limitation. In any case it's showed that, even with significant time performance differences and with magnetorquers experiencing high levels of saturation, both controllers are stable and settle. Moreover, it are hereafter presented the results for different initial conditions, resulting in aligning the angular velocity with the major axis of inertia at 0° and 180° as well as aligning the latter with the Earth's magnetic field lines at 0° and 180° as required.

6.2.1 Kane Damper results

The Kane Damper is addressed to damp the angular velocity components perpendicular to the spin axis. This is shown in Figures 6.8 and 6.9 for *positive* initial conditions, i.e. $\omega_0 = [0.6,\ -0.5,\ 0.7]^T \quad [rad/s]$.

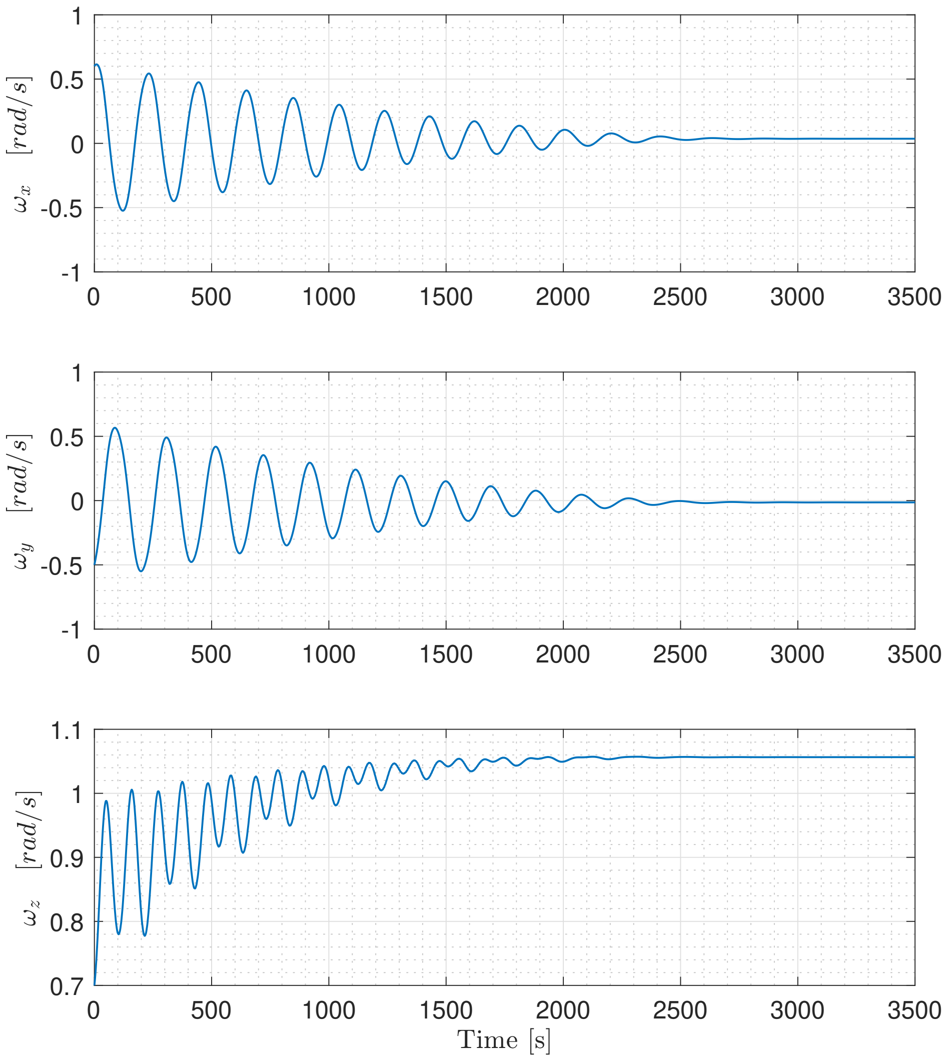

Figure 6.8: $\omega_x, \quad \omega_y, \quad \omega_z$ plot for *positive* initial conditions.

In particular, in Figure 6.8 we notice that the transverse components of angular velocity are damped, while the axial component of angular velocity increases. With this initial conditions the angular velocity settles in less than 3000 seconds.

In Figure 6.9 we see that the angular velocity vector aligns with the axis of maximum inertia (represented by the red dot) almost perfectly. In fact, evaluating the angle between the two vectors we have:

$$\theta_{\omega B} = 0.0922°$$

with final angular velocity:

$$\begin{aligned} \omega_n^b = & \quad [0.03598,\ -0.013903,\ 1.0565]^T \quad [rad/s] \\ |\omega_n^b| = & \quad 1.0572 \quad [rad/s]. \end{aligned}$$

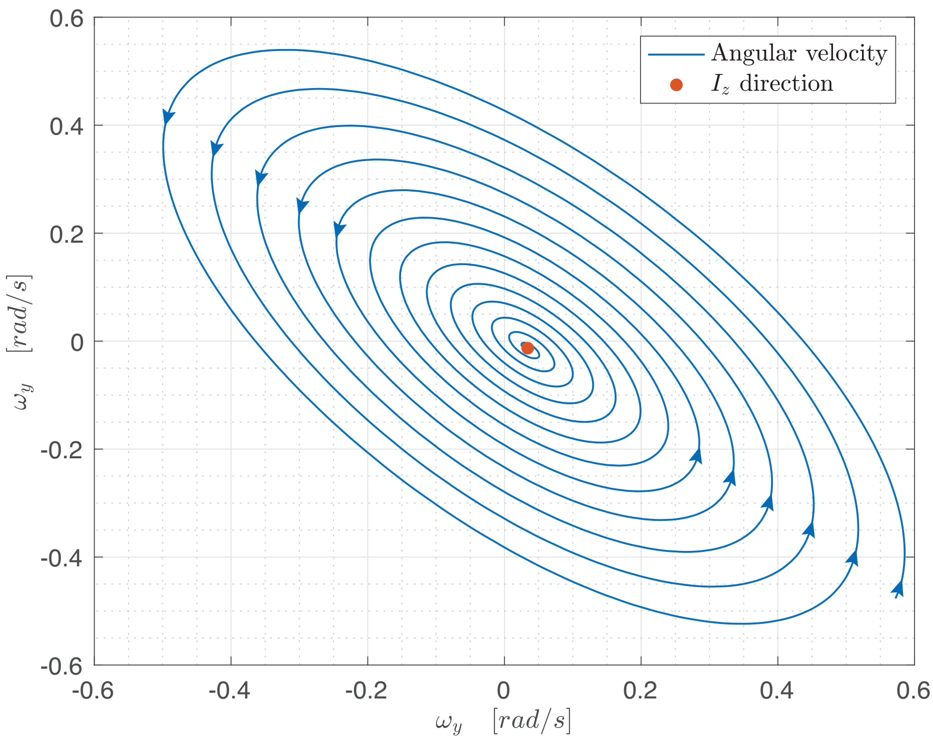

Figure 6.9: ω_x/ω_y plot for *positive* initial conditions.

The controller works with any initial conditions. For the sake of the simulation it is showed how it works with *negative* initial conditions, i.e. negative ω_z component, and how, in this case, it tents to spin counterclockwise but still aligns the angular velocity vector with the major axis of inertia. In this case we chose to use $\omega_0 = [-0.6,\ 0.5,\ -0.7]^T \quad [rad/s]$.
In Figure 6.10 we notice that also in this case the transverse components of angular velocity are damped, while the axial component of angular velocity decreases (increase in module).

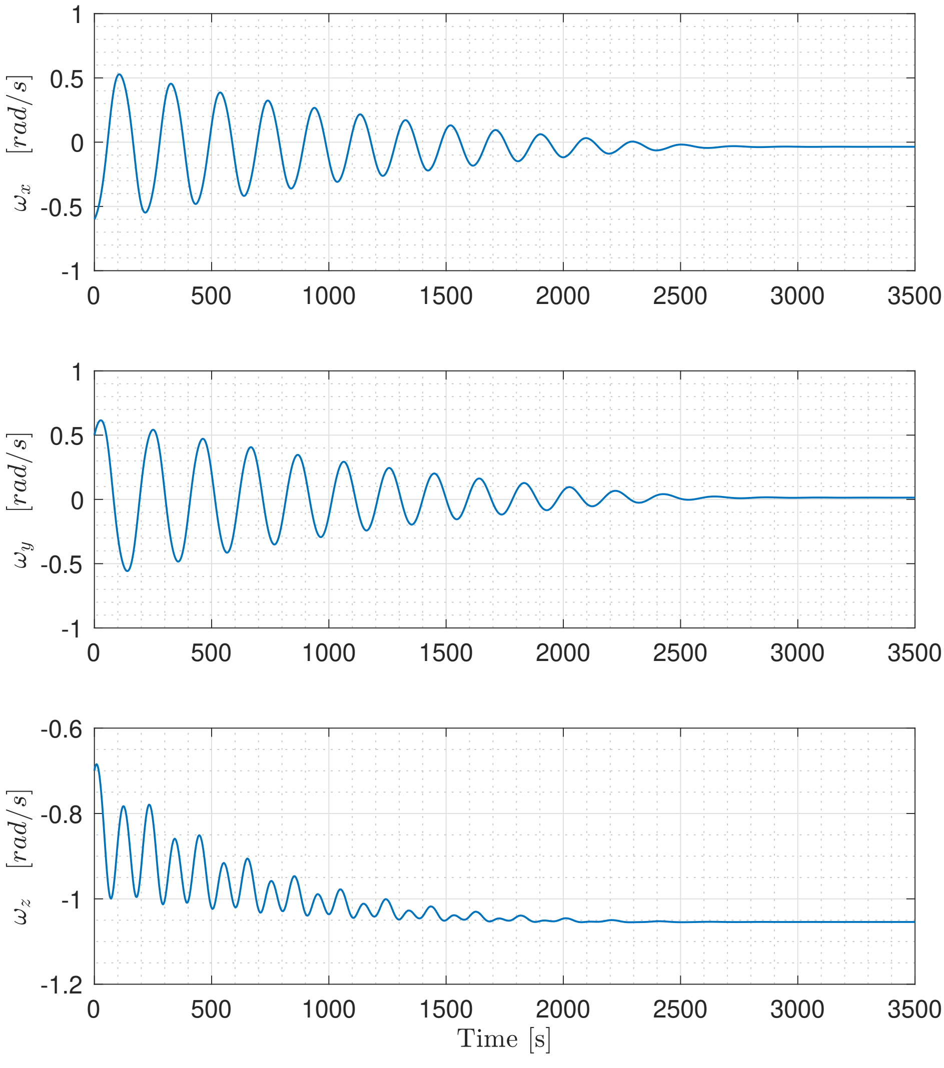

Figure 6.10: ω_x, ω_y, ω_z plot for *negative* initial conditions.

In Figure 6.11 we also see that the angular velocity vector aligns with the axis of maximum inertia following a counterclockwise path (instead of clockwise as before). The angle between the two vectors is, in this case:

$$\theta_{\omega B} = 179.995°$$

with final angular velocity:

$$\begin{aligned} \omega_n^b = & \quad [-0.035936,\ 0.01388,\ -1.0542]^T \quad [rad/s] \\ |\omega_n^b| = & \quad 1.0549 \quad [rad/s]. \end{aligned}$$

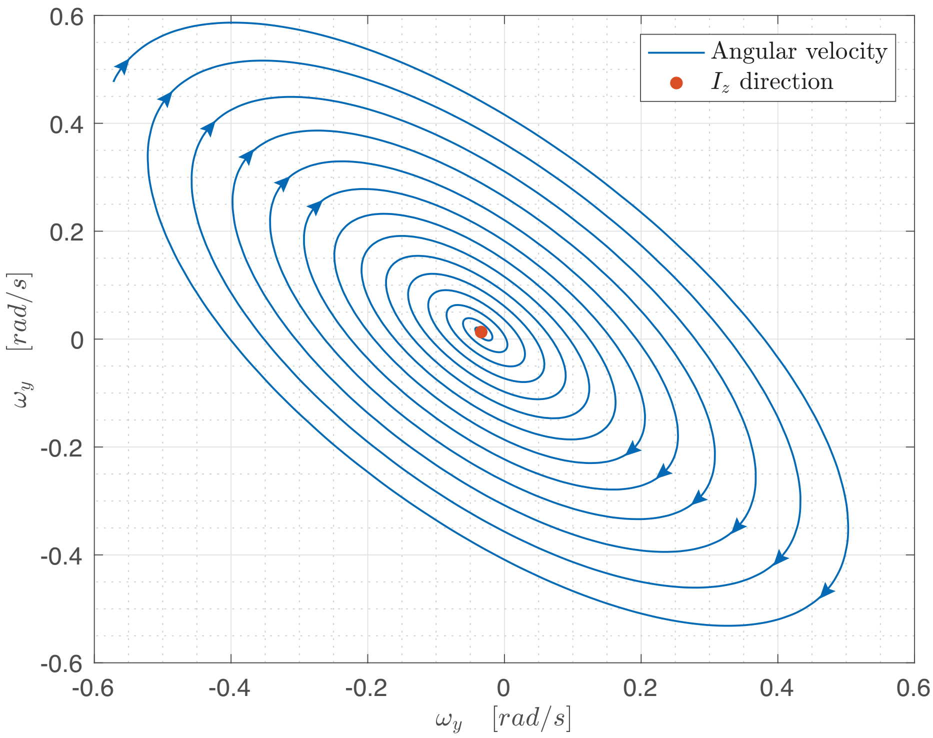

Figure 6.11: ω_x/ω_y plot for *negative* initial conditions.

6.2.2 Pointing controller results

The following results are related to the pointing controller which operates right after the previous, i.e. for *positive* initial conditions we have:

$$\omega_0^+ = [0.03598,\ -0.013903,\ 1.0565]^T \quad [rad/s]$$

and for *negative* initial conditions:

$$\omega_0^- = [-0.035936,\ 0.01388,\ -1.0542]^T \quad [rad/s]$$

In both cases the controller moves the spin axis towards the external magnetic field lines direction. This means that it will ideally lead to a final angle $\theta_{\omega B}$ of $0°$ of $180°$ depending on the initial condition, $\theta_{\omega B_0}$ that is the angle between the spin axis and the external magnetic field lines right after the first controller is shut down. Due to the oscillation of the external magnetic field we experience some oscillations. The frequency of the oscillation depends on the strength of the magnetorquers. Obviously, the greater the magnetic dipole they can generate, the fastest the response is. The two cases are shown in Figures 6.12 and 6.13

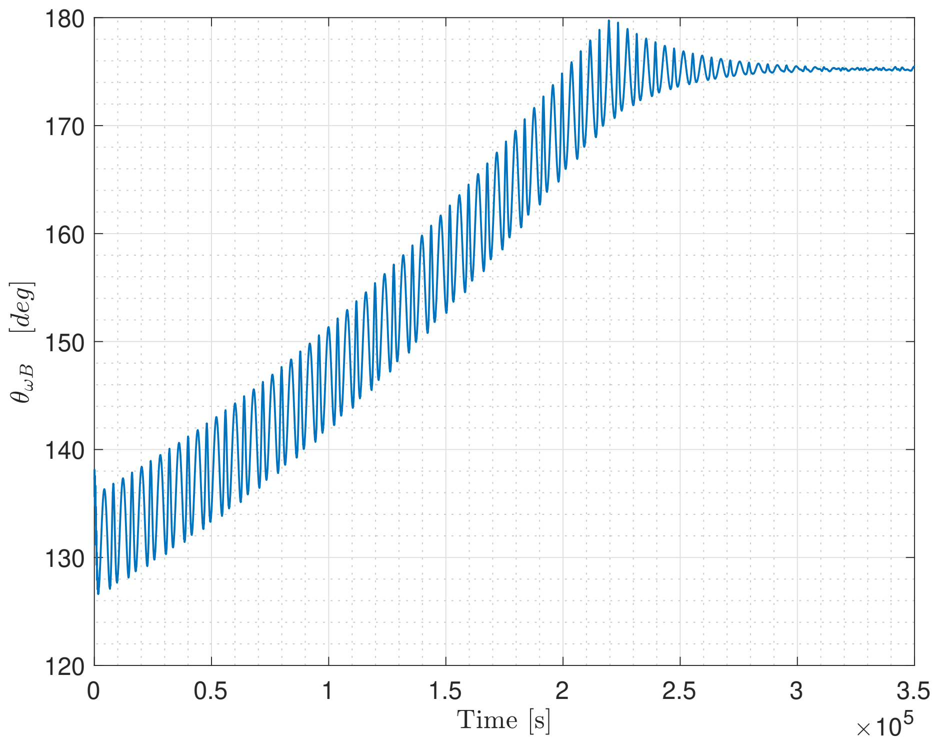

Figure 6.12: $\theta_{\omega B}$ plot for *negative* initial conditions, i.e. $\theta_{\omega B_0} \sim 138°$.

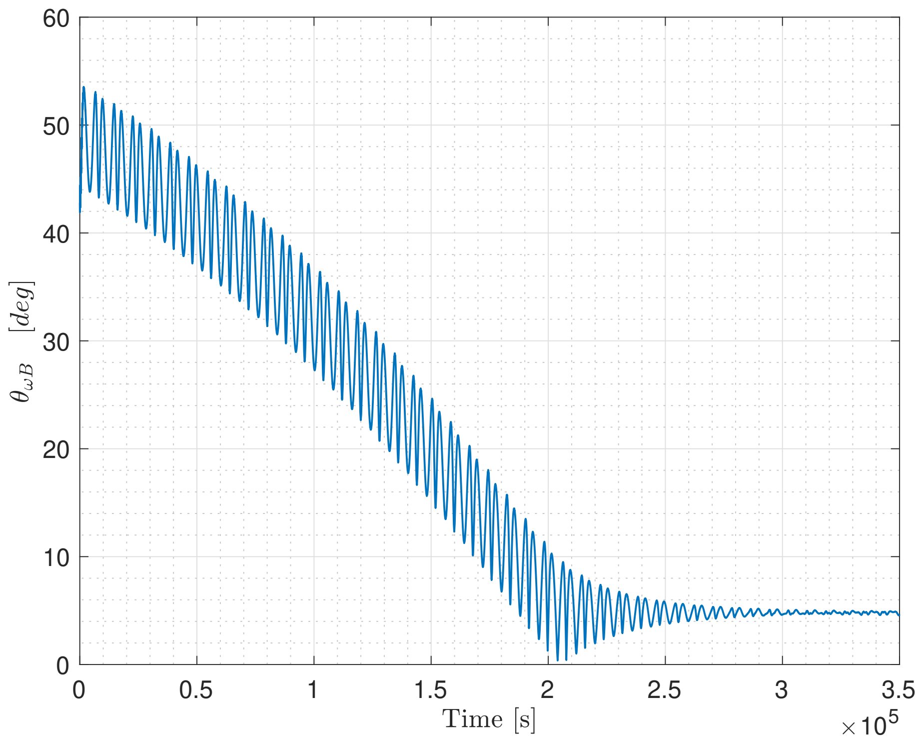

Figure 6.13: $\theta_{\omega B}$ plot for *positive* initial conditions, i.e. $\theta_{\omega B_0} \sim 44°$.

As we can see, the alignment is not perfect and in both cases we have a steady-state error of $\sim 5°$, in particular we have:

$$\theta_{\omega B} = 175.4187° \qquad e_{ss} = 4.5813°$$

for the motion with *negative* initial conditions, and

$$\theta_{\omega B} = e_{ss} = 4.6306°$$

for the motion with *positive* initial conditions. This, as said, is due to the weakness of the magnetic torques, and thus the generated magnetic dipole, as showed in (6.3). Hereafter is shown in Figure 6.14 that, if we get rid of the limitations on the z-axis magnetorquer's maximum magnetic dipole, the response is either faster and more accurate:

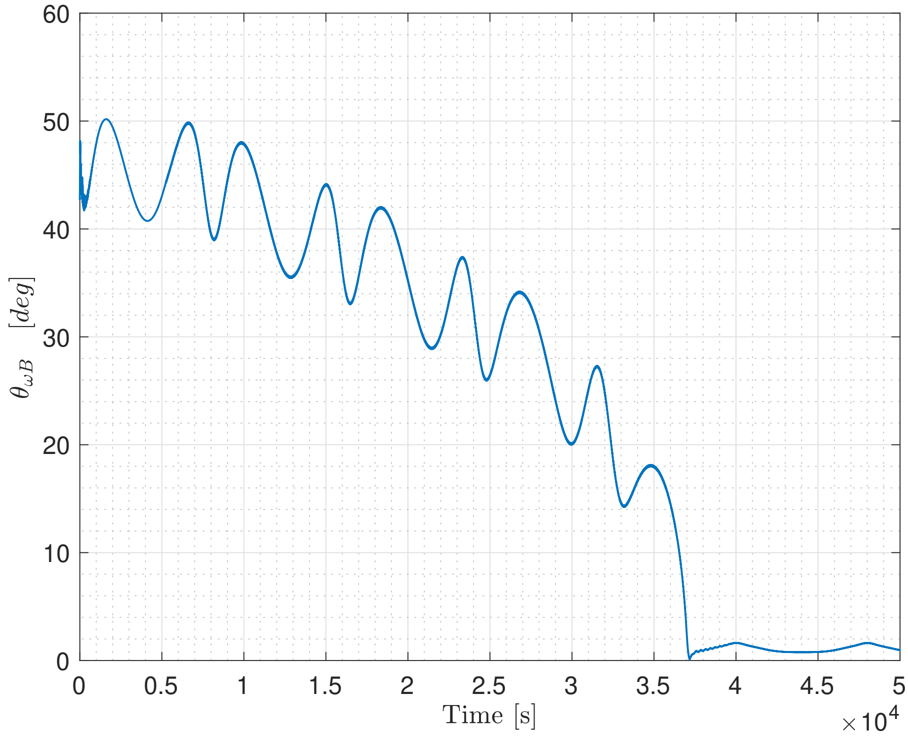

Figure 6.14: $\theta_{\omega B}$ plot for *positive* initial conditions, i.e. $\theta_{\omega B_0} \sim 44°$ without z-axis magnetorquer limitation.

As we can see from Figure 6.14 without the limitation on the maximum torque generated by the z-axis magnetorquer the final value is reached six times faster than with the limitation. Furthermore we also reduce the steady-state error:

$$\theta_{\omega B} = e_{ss} = 0.9720°$$

Chapter 7

Conclusion and Discussion

The developed nutation damper and pointing controllers perform as wanted. The simulations were run on random initial conditions and in any case they reach an acceptable level of accuracy being always stable, as highlighted in the stability section. In detail, the Kane Damper appears to be the most reliable in damping the initial nutation mode and both controllers are able to counteract the considered external disturbances. If the satellite is required to spin only in one direction of the spin axis another feature shall be added to the Kane Damper to increase the probability to spin about it's positive or negative major axis of inertia direction (as discussed in the stability section but not simulated as not required by the mission). Another improvement may come by a better design of the pointing controller. In particular, this may be adapted to an inertial-fixed pointing direction by adding a more accurate attitude determination system that may come by using a Kalman-filter on the Earth's magnetic field measurements or by using a sun sensor. Moreover, as we have seen in the last part of the results, the accuracy of the pointing controller is highly dependent on the strength of the spin-axis magnetorquer. Although performances may improve, it will weight on power consumption. This shall be taken into account in designing the magnetic torquer itself, if a different level of accuracy is required.

Bibliography

[1] Jasim Ahmed, Vincent T Coppola, and Dennis S Bernstein. "Adaptive asymptotic tracking of spacecraft attitude motion with inertia matrix identification". In: *Journal of Guidance, Control, and Dynamics* 21.5 (1998), pp. 684–691.

[2] Peter Al Hokayem and Eduardo Gallestey. "Lyapunov stability theory". In: *Nonlinear Systems and Control-Spring* (2015).

[3] Michael S Andrle and John L Crassidis. "Geometric integration of quaternions". In: *Journal of Guidance, Control, and Dynamics* 36.6 (2013), pp. 1762–1767.

[4] Giulio Avanzini and Fabrizio Giulietti. "Magnetic detumbling of a rigid spacecraft". In: *Journal of guidance, control, and dynamics* 35.4 (2012), pp. 1326–1334.

[5] PM Barba and TR Kane. "Effects of energy dissipation on a spinning satellite." In: *AIAA Journal* 4.8 (1966), pp. 1391–1394.

[6] L. J. Crotty and A. Samurkashian. *Alpha Project Overview*. Cornell University, Space System Design Studio, 2018.

[7] L. J. Crotty and A. Samurkashian. *Alpha System Requirement Review*. Cornell University, Space System Design Studio, 2018.

[8] Anton H De Ruiter, Christopher Damaren, and James R Forbes. *Spacecraft dynamics and control: an introduction*. John Wiley & Sons, 2012.

[9] Michael C Fu et al. *Handbook of simulation optimization*. Springer, 2016.

[10] Jan Tommy Gravdahl. "Magnetic attitude control for satellites". In: *Decision and Control, 2004. CDC. 43rd IEEE Conference on. Vol. 1. IEEE* (2004).

[11] S. Greenland and C. Clark. *CubeSat Platforms as an On-Orbit Technology Validation and Verification Vehicle*. Ed. by ESA Small Satellites and Services Symposium. Funchal, Madeira, Portugal, 2010.

[12] Peter C Hughes. *Spacecraft attitude dynamics*. Dover Publications, Inc., 2004.

[13] Hassan K Khalil. “Nonlinear systems, 3rd”. In: *New Jewsey, Prentice Hall* 9.4.2 (2002).

[14] Wiley J. Larson and James R. Wertz. *Space mission analysis and design.* Microcosm, 1992.

[15] Wilbur R LePage. *Complex variables and the Laplace transform for engineers.* Courier Corporation, 2012.

[16] Frederick A. Leve, Brian J. Hamilton, and Mason A. Peck. *Spacecraft Momentum Control Systems.* Ed. by Springer. Vol. Vol. 1010. 2015.

[17] F Landis Markley and John L Crassidis. *Fundamentals of spacecraft attitude determination and control.* Vol. 33. Springer, 2014.

[18] Anh-Tuan Nguyen, Sigrid Reiter, and Philippe Rigo. “A review on simulation-based optimization methods applied to building performance analysis”. In: *Applied Energy* 113 (2014), pp. 1043–1058.

[19] Michael C Norman, Mason A Peck, and Daniel J O’shaughnessy. “In-orbit estimation of inertia and momentum-actuator alignment parameters”. In: *Journal of Guidance, Control, and Dynamics* 34.6 (2011), pp. 1798–1814.

[20] Ajayi Michael Oluwatosin, Yskandar Hamam, and Karim Djouani. “"Attitude control of a CubeSat in a circular orbit using magnetic actuators."” In: *IEEE* (2013).

[21] Hamed Shahmohamadi Ousaloo and Ali Badpa. “Magnetic attitude control system for spin stabilized satellite”. In: *Electrical Engineering (ICEE), 2012 20th Iranian Conference on.* IEEE. 2012, pp. 1029–1034.

[22] M Yu Ovchinnikov et al. “Magnetic attitude control systems of the nanosatellite TNS-series”. In: *Small Satellites for Earth Observation: Selected Proceedings of the 5th International Symposium of the International Academy of Astronautics, Berlin, April 4-8 2005.* Walter de Gruyter. 2005, p. 337.

[23] DS Roldugin and P Testani. “Spin-stabilized satellite magnetic attitude control scheme without initial detumbling”. In: *Acta Astronautica* 94.1 (2014), pp. 446–454.

[24] Masamichi Shigehara. “Geomagnetic attitude control of an axisymmetric spinning satellite”. In: *Journal of spacecraft and rockets* 9.6 (1972), pp. 391–398.

[25] Jean-Jacques E Slotine, Weiping Li, et al. *Applied nonlinear control.* Vol. 199. 1. Prentice hall Englewood Cliffs, NJ, 1991.

[26] Martin Walt. *Introduction to geomagnetically trapped radiation.* Cambridge University Press, 2005.

[27] James R. Wertz. *Spacecraft Attitude Determination and Control*. Springer Netherlands, 1978.

Acknowledgements

First of all I want to thank prof. Sabrina Corpino, for inspiring me about space and for supporting me during my studies and my thesis work, as well as giving me the opportunity to join a student Team in which I improved my knowledge in space systems. Of course I'd like to thank prof. Mason Peck from Cornell University, for supporting me during my thesis and for giving me his knowledge, without which this work couldn't be done. I also take the opportunity to thank both Polito CubeSat Team and Alpha CubeSat Team, in which I experienced interesting experience and cultural exchange moments. Of course I thank my parents, Anna and Angelo, for supporting me during all my academic path, and my sister Paola for tolerating me during those last years. Finally I must thank all the friends and colleagues with which I shared good and bad moments, academic and not, and most of which became part of my days and with which I realized a friendship that goes beyond the study. In particular I should mention Gigi "the other" friends and the Opera. I should also include Paola, who is been giving me the strength to go on for years, who is been waiting for me and became a real part of my days and my life.
Farewell Politecnico.

Ringraziamenti

Voglio ringraziare innanzitutto la prof. Sabrina Corpino, per avermi trasmesso la passione per lo spazio e per avermi supportato nel mio percorso didattico e di tesi, nonchè per la possibilità di far parte di un Team di studenti nel quale ho migliorato le mie conoscenze sui sistemi spaziali. Ringrazio senz'altro il prof. Mason Peck dalla Cornell University per avermi seguito e supportato durante il mio lavoro di tesi e per avermi trasmesso le sue conoscenze, senza le quali tale lavoro non sarebbe stato possibile. Colgo l' occasione per salutare e ringraziare il Polito CubeSat Team e l' Alpha CubeSat Team, nei quali ho vissuto esperienze interessanti e momenti di scambio culturale. Sicuramente ringrazio i miei genitori Anna ed Angelo, per avermi supportato in tutto il percorso universitario, e mia sorella Paola per avermi sopportato durante questi ultimi anni. Infine non posso non salutare e ringraziare tutti gli amici e colleghi con cui ho condiviso gioie e sofferenze, didattiche e non, molti dei quali sono entrati a far parte della mia vita quotidiana e con i quali ho stretto amicizie che vanno ben al di lá dello studio. Una particolare menzione voglio riservarla agli amici di Gigi l'altro ed all'Opera che mi ha accolto in numerose giornate di studio. Non posso non includere nei ringraziamenti Paola, che da anni mi dá forza e mi aiuta ad andare avanti, che mi ha aspettato per mesi ed è diventata parte integrante delle mie giornate e della mia vita.
Addio Politecnico.